



CrossMark  
click for updates

Cite this: *RSC Adv.*, 2015, 5, 69086

# Microfabricated electrochemical pH and free chlorine sensors for water quality monitoring: recent advances and research challenges

Yiheng Qin, Hyuck-Jin Kwon, Matiar M. R. Howlader\* and M. Jamal Deen\*

Continuous, real-time monitoring of the level of pH and free chlorine in drinking water is of great importance to public health. However, it is challenging when conventional analytical instruments, such as bulky pH electrodes and expensive free chlorine meters, are used. These instruments have slow response, are difficult to use, prone to interference from operators, and require frequent maintenance. In contrast, microfabricated electrochemical sensors are cheaper, smaller in size, and highly sensitive. Therefore, these sensors are desirable for online monitoring of pH and free chlorine in water. In this review, we discuss different physical configurations of microfabricated sensors. These configurations include potentiometric electrodes, ion-sensitive field-effect transistors, and chemo-resistors/transistors for electrochemical pH sensing. Also, we identified that micro-amperometric sensors are the dominant ones used for free chlorine sensing. We summarized and compared the structure, operation/sensing mechanism, applicable materials, and performance parameters in terms of sensitivity, sensing range, response time and stability of each type of sensor. We observed that novel sensor structures fabricated by solution processing and operated by smart sensing methodologies may be used for developing pH and free chlorine sensors with high performance and low cost. Finally, we highlighted the importance of the concurrent design of materials, fabrication processes, and electronics for future sensors.

Received 13th June 2015  
Accepted 4th August 2015

DOI: 10.1039/c5ra11291e

[www.rsc.org/advances](http://www.rsc.org/advances)

Department of Electrical and Computer Engineering, McMaster University, 1280 Main Street West, Hamilton, ON, L8S 4K1, Canada. E-mail: [mrhowlader@ece.mcmaster.ca](mailto:mrhowlader@ece.mcmaster.ca); [jamal@mcmaster.ca](mailto:jamal@mcmaster.ca)

## 1 Introduction

The quality of water is determined by bio-physico-chemical parameters including, but not limited to pH, free chlorine concentration, turbidity, dissolved oxygen, conductivity, organic carbon, and some types of microorganisms.<sup>1</sup> Among



Yiheng Qin is currently pursuing a Ph.D. degree in Department of Electrical and Computer Engineering at McMaster University, Hamilton, Canada. He received his B.S. degree in Electronics Science and Technology (Microelectronics Technology) from Southwest Jiaotong University, Chengdu, China, in 2009, and received his M.S. degree in Microtechnology from Chalmers University of Technology,

Göteborg, Sweden, in 2011. His research interests include nano-integration technologies, with a focus on the use of organic and inorganic materials in biomedical and environmental sensing applications.



Hyuck Jin Kwon received a B.S. and M.S. degrees in Agricultural Engineering from Seoul National University, in Seoul, Korea, in 2000 and 2002, and his Ph.D. degree in Agricultural and Biosystems Engineering from University of Arizona, Tucson, AZ, USA, in 2011, respectively. Dr Kwon is currently a postdoctoral research fellow in the Department of Electrical and Computer Engineering at

McMaster University, Hamilton, ON, Canada. His research focuses on design of microfluidic sensors by computational fluid dynamics and development of a low cost sensor for health and environmental applications.

them, the pH value and free chlorine concentration is critical to the natural environment and our health. The pH of an aqueous solution is defined as the negative common logarithm of the molar concentration of hydronium ions ( $\text{H}_3\text{O}^+$ ), given by  $\text{pH} = -\log[\text{H}_3\text{O}^+]$ . The usual range of pH is 0 to 14, where pH = 7 is the neutral value, pH 7 denotes a basic solution.<sup>2</sup>

According to the World Health Organization (WHO), the recommended optimum level of pH for drinking water is in the range of 6.5 to 9.5.<sup>3</sup> The Canadian government has a narrower range of 6.5 to 8.5.<sup>4</sup> If the pH of water in the distribution system is outside the recommended range, it may indicate some problems in water treatment and could eventually affect our health. For example, the leaching and nitrification of water is indicated by lower pH values;<sup>5</sup> the presence of microorganisms in water changes the pH by producing acidic or basic metabolic species;<sup>6</sup> accidental spills of disinfecting chemicals and breakdown of treatment system can even result in extreme pH values (pH outside the range of 4 to 10).<sup>7</sup> Water with unusual pH values may have abnormal odor and taste. It may cause gastrointestinal irritation,<sup>8</sup> corrosion of metal pipes,<sup>9</sup> and indicate inefficient disinfection.<sup>10</sup> Therefore, pH has to be continuously monitored at all stages of water treatment.<sup>11</sup>

On the other hand, chlorine is introduced into the water treatment system for disinfection due to its capability to bond with and destroy the outer surfaces of bacteria and viruses.<sup>12</sup> However, chlorine should be used in a controlled manner to safely and effectively disinfect water. The WHO states that 2 to 3 ppm chlorine should be added into water to get an effective disinfection and acceptable residual concentration.<sup>13</sup> In US standards, the maximum concentration of residual chlorine in drinking water is 4 ppm.<sup>14</sup> Also, the suggested concentration for free chlorine in a well-maintained swimming pool is 1.5 to 2 ppm.<sup>15</sup>

Underfeeding of chlorine may result in incomplete disinfection that threatens public health. Overfeeding may generate objectionable order and increase the level of trihalomethanes

(suspected carcinogens) in the treated water.<sup>16</sup> Moreover, chlorine is a costly chemical whose production requires a large amount of energy (around 3000 kWh electricity is needed for producing 1 ton chlorine from brine).<sup>17</sup> As a result, the free chlorine level in water is a critical parameter that should be monitored routinely and frequently.

Traditional analytical approach for water quality monitoring consists of multiple steps: water sampling, sample transportation to laboratories, and laboratory analysis.<sup>18</sup> This approach is time-consuming, expensive and laboratory-dependent. Also, the results are easily affected by anthropogenic interference as well as long-term storage of the water samples.<sup>19,20</sup> For example, conventional glass pH electrodes are brittle, large in dimensions, slow in response, costly, and they need regular maintenance such as calibration and refilling of the reference buffer solution.<sup>21</sup> For free chlorine monitoring, the commonly used *N,N*-diethyl-*p*-phenylenediamine (DPD) analyzers have high sensitivity and can provide accurate results in a limited detection range if they are calibrated frequently. However, such analyzers rely on expensive optical instruments, generate environmentally harmful chemicals, are prone to the interference of certain iron and manganese species, and are difficult to miniaturize.<sup>22</sup> Therefore, alternative sensing technologies need to be developed to address these challenges.

The utilization of accurate, easy-to-use, small-footprint and inexpensive sensors is an attractive alternative approach. Recent developments in microfabrication technologies enable the realization of such sensors. The advantages of the microfabrication technologies include the precise control of material surface morphologies (such as roughness), the ability to tailor material properties (such as conductivity), and the reduction of materials used. Also, micro-scale sensors can be integrated with other components to create high-functionality integrated systems for automatic operation.<sup>23,24</sup>

There are reports of several hydrogel-based sensors using micro chemical-mechanical transducers for the measurement



*Matiar M. R. Howlader received a B. Sc. Eng. degree in Electrical and Electronic Engineering from Khulna University of Engineering and Technology, in Khulna, Bangladesh, in 1988, and his M.S. and Ph.D. degrees in Nuclear Engineering from Kyushu University, Fukuoka, Japan, in 1996 and 1999, respectively. Currently, Dr Howlader is leading the nano-bonding and packaging research*

*group in the Department of Electrical and Computer Engineering at McMaster University, Hamilton, ON, Canada. His research focuses on the nano-integration of bio-micro-opto-electromechanical systems, sensor systems and implantable systems for health and environmental applications.*



*M. Jamal Deen received the Ph.D. degree in electrical engineering and applied physics from Case Western Reserve University, Cleveland, OH, in 1985. His Ph.D. dissertation was focused on the design and modeling of a new CARS spectrometer for dynamic temperature measurements and combustion optimization in rocket and jet engines, and was sponsored by NASA, Cleveland.*

*He is currently a Distinguished University Professor, Senior Canada Research Chair in information technology and Director of the Micro- and Nano-Systems Laboratory at McMaster University. His research interests include microelectronics/nanoelectronics, optoelectronics, and nanotechnology and their emerging applications.*

of pH.<sup>25–28</sup> However, these sensors are not widely studied and are more difficult to implement due to their brittle structures and long response time (hundreds of minutes). On the other hand, micro-optical sensors are highly accurate and sensitive, but their sensing range is limited and linearity is poor. Also, the components for optical sensors such as lasers and detectors are expensive,<sup>29–32</sup> and usually, the sensors require chemical reagents for the measurement.<sup>33</sup> Therefore, chemo-mechanical and optical sensors are challenging to implement for continuous, low-cost and easy-to-use water quality monitoring. The advantages of the microfabricated electrochemical sensors over other types of sensors and analytical methods include the following.

- Wider sensing range and faster response with comparable sensitivity.
- Easier integration with microelectronic components for automatic operation.
- Smaller dimensions and higher structural compatibility with existing water distribution systems.
- Better compatibility with additive fabrication technologies.
- Lower cost so that they can be deployed more widely.

Because of these advantages, many researchers are investigating microfabricated electrochemical pH sensors. Banna *et al.* provided a general review on sensing technologies for measurement of various water quality parameters.<sup>11</sup> Miao *et al.* briefly listed the applications of new materials and techniques for different types of pH sensors.<sup>21</sup> Vonau and Guth compared miniaturized solid-state pH electrodes made from metal oxides.<sup>34</sup> Kurzweil summarized metal oxides as pH sensors based on ion-exchange mechanisms.<sup>35</sup> Korostynska *et al.* reviewed the development of polymer-based pH sensors, including those for *in vivo* applications.<sup>8,36</sup> Shinwari *et al.* reviewed microfabricated reference electrodes for sensing applications.<sup>37</sup> In addition, there are several review papers in which micro-scale chemical and biological sensors fabricated using organic materials are described.<sup>38–44</sup> However, to the best of our knowledge, the recent development in microfabricated electrochemical pH sensors has not yet been comprehensively reviewed, and a review of electrochemical-based microfabricated free chlorine sensors was not found.

This review provides an up-to-date discussion of microfabricated electrochemical pH and free chlorine sensors with different sensing configurations and with a focus on water quality monitoring. A brief introduction on conventional pH and free chlorine monitoring techniques is presented in Section 2. In Section 3, we discuss the sensing mechanisms along with the structures, materials and performance parameters of the microfabricated electrochemical pH sensors. They are categorized into potentiometric electrodes, ion-sensitive field-effect transistors (ISFETs), and chemo-resistor/transistors. In Section 4, we consider amperometric sensor as the major type of small-size, free chlorine sensors. The recently developed free chlorine sensors are reviewed in terms of their configurations, sensing mechanisms, materials, and performance. At the end of Sections 3 and 4, we state the challenges in developing future pH and free chlorine sensors. We also compare the advantages and disadvantages of each type of sensors, along with two

comprehensive lists of recently reported micro-electrochemical pH and free chlorine sensors. In Section 5, conclusions and future perspectives are provided.

## 2 Conventional monitoring techniques for pH and free chlorine

### 2.1 pH monitoring

Conventional technologies for pH measurement for water quality monitoring are mainly depending on glass electrode-based pH meters, which were invented by Arnold Beckman in 1934 and commercialized in 1936.<sup>45</sup> The first pH meter included a glass-indicating electrode that was developed by F. Haber and Z. Klemensiewicz in 1909 and integrated with a vacuum tube amplifier.<sup>46</sup> In the next several decades, different types of pH sensors emerged, and they could be mainly categorized into chemo-mechanical sensors, electrochemical sensors, and optical sensors.<sup>11</sup> Even today, the most commonly used pH sensors are still the glass-membrane-based electrochemical electrodes.

A typical glass electrode consists of a bulb made from a specific glass (for example, a glass containing lithium or sodium ions), internal solution (usually 0.1 M hydrochloride acid or buffered chloride solution), internal electrode (usually silver/silver chloride, Ag/AgCl, or calomel electrode), and glass or plastic electrode body.<sup>35</sup> During pH measurement, the outer surface of the bulb is hydrated by forming a silicate skeleton layer, which is designed to be selectively permeable to H<sub>3</sub>O<sup>+</sup>. Similarly, a hydrated layer is created on the inner side of the bulb. The amount of charges at the inner side is proportional to the amount of permeated H<sub>3</sub>O<sup>+</sup> at the outer side (relating to the concentration of H<sub>3</sub>O<sup>+</sup> in the external solution). The potential difference across the glass bulb membrane ( $E$ ) is given by Nernst equation:<sup>47</sup>

$$E = E^0 + \frac{2.303RT}{nF} \log[\text{H}_3\text{O}^+] \quad (1)$$

where  $E^0$  is the standard cell potential, which is a function of the standard potential of the internal reference electrode (relative to standard hydrogen electrode) and the resistivity of the internal solution.  $R$  is the gas constant (8.314 J K<sup>-1</sup> mol<sup>-1</sup>),  $T$  is the absolute temperature,  $n$  is the valence of the ion (1 for H<sub>3</sub>O<sup>+</sup>),  $F$  is Faraday's constant (9.649 × 10<sup>4</sup> C mol<sup>-1</sup>), and [H<sub>3</sub>O<sup>+</sup>] is the ion activity (relating to the molar concentration of H<sub>3</sub>O<sup>+</sup>). At 25 °C, the electrode potential as a function of solution pH is:

$$E = E^0 - 0.05916\text{pH} \quad (2)$$

which shows the ideal pH sensitivity of the glass electrode is 59.16 mV per pH. This value is known as the Nernst slope in the pH-voltage plot and has been treated as the reference value in the development of novel pH sensors.

### 2.2 Free chlorine monitoring

Free chlorine in water consists of two chemicals: hypochlorous acid (HOCl) and hypochlorite ion (OCl<sup>-</sup>). When chlorine gas is introduced into water for disinfection, HOCl is produced:<sup>48</sup>

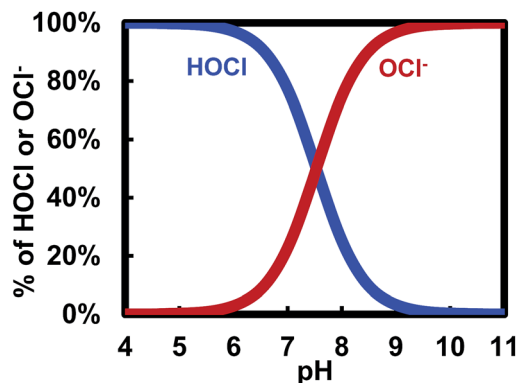
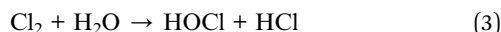
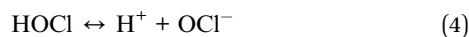


Fig. 1 Distribution of hypochlorous acid and hypochlorite ion in water at different pH values.



where HOCl is a weak acid and can be partially dissociated into  $\text{H}^+$  and  $\text{OCl}^-$  in water:



Thus, at a certain temperature, the percentage distribution of HOCl and  $\text{OCl}^-$  is a function of the concentration of  $\text{H}^+$  ( $\text{H}_3\text{O}^+$ ), which is the pH of the solution (Fig. 1). This relation can be generally expressed by:

$$\log \frac{[\text{OCl}^-]}{[\text{HOCl}]} = \log K_a + \text{pH} \quad (5)$$

where  $[\text{OCl}^-]$  and  $[\text{HOCl}]$  are the equilibrium concentrations of  $\text{OCl}^-$  and HOCl, respectively, and  $K_a$  is the dissociation constant of HOCl (around  $10^{-7.53}$  at  $25^\circ\text{C}$ ).<sup>49</sup> One can measure the solution pH together with the concentration of either HOCl or  $\text{OCl}^-$  to obtain the level of free chlorine. Two commonly used analytical methods for free chlorine monitoring are colorimetric and electrochemical analysis, including: absorptiometry methods using DPD,<sup>50</sup> *o*-tolidine<sup>51</sup> or other chemicals;<sup>52–54</sup> iodometric titration;<sup>55</sup> chromatography;<sup>56</sup> chemiluminescence;<sup>57</sup> and amperometric methods.<sup>58,59</sup>

The DPD-based absorptiometry method has been extensively used owing to its high sensitivity. When the solution pH is around 7, free chlorine oxidizes DPD to form a colored magenta compound.<sup>50</sup> The color can be photometrically read out to determine the amount/concentration of chlorine. This method usually can detect free chlorine in the concentration range of 0 to 5 ppm with an accuracy of 0.04 ppm. It has been considered as a standard analytical approach and approved by the United States Environmental Protection Agency for online monitoring of free chlorine.<sup>22</sup>

### 3 Microfabricated electrochemical pH sensors

In the literature, more than seven mechanisms were described to explain the working principles of solid-state electrochemical pH sensors.<sup>60–62</sup> These mechanisms include:

(1)  $\text{H}_3\text{O}^+$  ion exchange in a membrane rich in hydroxyl groups ( $-\text{OH}$ ). It is the mechanism for conventional glass electrodes.

(2) Redox equilibrium involving  $\text{H}_3\text{O}^+$  ions between a metal and its oxides, such as an antimony electrode.

(3) Redox equilibrium involving  $\text{H}_3\text{O}^+$  ions between metal oxides with different metal valences, such as iridium oxide ( $\text{IrO}_x$ ) electrodes.

(4) Redox equilibrium involving a solid-phase material and  $\text{H}_3\text{O}^+$  ions, whose hydrogen content can be changed by applying an electrical current, such as conductive polymer-based electrodes.

(5) Steady-state corrosion of the electrode material by  $\text{H}_3\text{O}^+$  ions, but this is not suitable for practical uses.

(6) Change of surface potential of a solid-state material due to the pH change of the contacting solution, based on the site-dissociation and double-layer models at the solid-liquid interface. Such theory was applied in transistor-based pH sensors.

(7) Variation of electrical properties (such as resistivity) of a material with changes in the pH of the solution.

Based on these transduction mechanisms, different configurations of pH sensors were developed. In addition to these methods, other mechanisms and sensor structures, such as voltammetric,<sup>63,64</sup> impedimetric,<sup>65</sup> and diode-based sensors,<sup>66</sup> were reported. In subsection 3.1 to 3.3, we focus on the more widely reported pH sensors structured as potentiometric electrodes, ISFETs, and chemo-resistor/transistors.

#### 3.1 Potentiometric sensor

**3.1.1 Sensor configuration and sensing mechanism.** A typical potentiometric sensor has a two-electrode structure, one electrode being the sensing electrode and the other, the reference electrode with Ag/AgCl is the most commonly used reference electrode in micro-scale pH sensors.<sup>67–69</sup> When both electrodes contact the solution, the electrical potential difference between them is measured to determine the  $\text{H}_3\text{O}^+$  concentration in the solution. Fig. 2 shows a schematic of a potentiometric pH sensor and its possible sensing mechanisms.

For potentiometric sensors, two possible mechanisms for pH sensing were observed: redox reactions and ion-selective permeation. First, if the material on the sensing electrode has redox reactions with  $\text{H}_3\text{O}^+$ , then a potential difference is generated by the free energy change as reversible chemical reactions approaching their equilibrium conditions.<sup>67</sup> Second, if the sensing material acts as an ion-selective membrane, the concentration gradient of ions across the membrane also generates a potential difference. For both cases, the potential can be quantitatively determined by the Nernst equation, as discussed previously in Section 2. Ideally from eqn (2), the change of 1 pH unit at  $25^\circ\text{C}$  will result in a 59.16 mV change in the potential difference between the sensing and reference electrodes.

The potentiometric configuration is simple when compared to other sensor structures. It only requires two electrodes and no power supply is needed for its operation. Thus, the

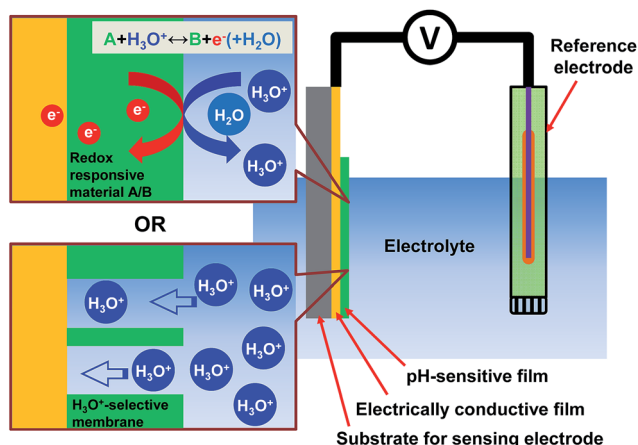


Fig. 2 Schematic of a potentiometric pH sensor and its possible sensing mechanisms.

dimensions of potentiometric sensors can be reduced. The potential difference between the sensing and reference electrodes is normally hundreds of millivolts, which can be easily read out by inexpensive, commercial voltmeters. Therefore, potentiometric sensors are widely used in laboratories for the characterization of newly developed pH sensitive materials.

**3.1.2 Applicable materials and sensor performance.** The electrical conductivity of pH sensitive material being used at the potentiometric sensing electrode should not be low for the transfer of electrons generated by the redox reactions. Thus, conductive and semiconductive metal oxides and organic materials are used. Several of these are now described.

$\text{IrO}_x$  was reported as an outstanding material for pH measurement over wide ranges, with fast responses, and high durability and stability.<sup>70</sup> Several approaches for the preparation of microfabricated  $\text{IrO}_x$  electrodes were used. They include: thermal oxidation of iridium (Ir),<sup>71</sup> electroplating,<sup>72,73</sup> anodization,<sup>74</sup> sputtering,<sup>66,75</sup> and sol-gel processing.<sup>76</sup> Generally, the  $\text{IrO}_x$  electrodes have near-Nernstian response (59.16 mV per pH), because the amount of transferred electrons equals to the amount of reacted  $\text{H}_3\text{O}^+$ . However,  $\text{IrO}_x$  prepared by electrochemical deposition showed super-Nernst response (pH sensitivity greater than 59.16 mV per pH), with a sensitivity of around 70 mV per pH.

To explain the super-Nernstian response, it is proposed that the electrochemically deposited  $\text{IrO}_x$  can become hydrated in an aqueous environment and contains Ir ions with different valences (+3 and +4).<sup>72,73</sup> If  $\text{IrO}_x$  is fully hydrated, the redox reaction is



This reaction shows that every 3 hydrogen ions will lead to the transfer of 2 electrons. As a result, the pH response for this reaction is  $(3/2)(RT/F) = 88.74$  mV per pH at 25 °C. If  $\text{IrO}_x$  is partially hydrated, thus a Nernst slope between 59.16 and 88.5 mV per pH should be obtained. The  $\text{IrO}_x$  electrodes can cover a pH sensing range between 1 and 13 with short response times. It is worth noting that a less porous sensing surface gives faster

response.<sup>76</sup> For example, nano-porous  $\text{IrO}_x$  exhibited a response time of 100 s while that of a dense film is less than 2 s.

Other metal oxides have also been studied, but their pH sensitivities were not as high as  $\text{IrO}_x$ . Nano-copper oxide,<sup>77</sup> cobalt oxide,<sup>78</sup> tungsten oxide<sup>79</sup> were synthesized by hydrothermal growth and their pH sensitivities were 28, 58.5, and 56.7 mV per pH, respectively. Sputtered ruthenium oxide sensors were reported with a super-Nernst response of about 69 mV per pH.<sup>80</sup> However, the explanation for this phenomenon of was not given.

A super-Nernst response of 84 mV per pH was achieved with  $\beta$ -phase lead dioxide nanoparticles deposited electrochemically.<sup>81</sup> The pH sensing range of this sensor was from 0.12 to 13, which is the widest in recent publications. The superior response was attributed to the multiple oxidation states of lead oxide, which was similar to the electrochemically deposited  $\text{IrO}_x$ . In addition, palladium oxide (PdO) generated from solution-processed palladium (Pd) precursor was tested and a pH sensitivity around 65 mV per pH was obtained. Also, because this sensor was prepared at a low temperature (200 °C), it could potentially be integrated with polymeric substrates to reduce the cost of the pH sensors.<sup>82</sup>

In addition to metal oxides, many conductive polymers (CPs) were also fabricated as potentiometric electrodes. Their pH sensitivity is attributed to their acidic and/or basic functional groups, which can be protonated or deprotonated at different pH levels.<sup>42</sup> Deprotonation of CPs results in a decrease of charge carrier density along the polymer chains, which alters the materials' redox, electrical and optical properties. Two widely studied CPs are polyaniline (PANI) and polypyrrole (PPY). The amino groups in their polymer chains have affinity towards  $\text{H}_3\text{O}^+$ . Hence, PANI and PPY thin films can be considered as  $\text{H}_3\text{O}^+$  permeable membrane and a Nernst response was observed in pH buffers.<sup>83–85</sup> Another contributor to the Nernst response of CP-based pH sensors is the redox equilibrium, similar to metal oxide-based sensors.

PANI electrodes prepared by electropolymerization showed a slight super-Nernst response (62.4 mV per pH) in the pH range of 2 to 9.<sup>83</sup> Due to the reliable near-Nernst performance and fast response time <25 s in the physiological pH range (3 to 8), PANI-based wearable sensors were used to measure the pH values of bio-fluids.<sup>86,87</sup> Compared to PANI-based sensors, PPY was tested in a wider pH range of 2 to 12, but a lower sensitivity (~50 mV per pH) was measured.<sup>84,85,88</sup> Such sensors were shown to be stable over 30 days.

Considering other organic materials, parylene-C normally used as an insulating material, also displayed a pH sensitivity of 16.3 mV per pH between pH of 4 and 10.<sup>89</sup> Although the sensitivity of parylene-C was low, its process compatibility with existing microelectronics fabrication technologies makes it suitable for low-cost applications.<sup>90–93</sup> Carbon nanotubes (CNTs) were also evaluated as a pH sensitive material with a Nernst response.<sup>94</sup>  $\text{H}_3\text{O}^+$  and  $\text{OH}^-$  can dope CNT walls by behaving as electron acceptors and donors. Thus, the Fermi level of CNTs changes with the pH value, leading to a shift of the measured open-circuit potential.

### 3.2 ISFET

#### 3.2.1 Sensor configuration and sensing mechanism: ISFET.

The ISFET was described by Bergveld in 1970, its configuration was a metal-oxide-semiconductor field-effect transistor (MOSFET) with the gate separated from the chip by the solution to be monitored. The gate metal was replaced by a reference electrode and the dielectric layer is normally critical to the sensing performance (Fig. 3).<sup>44,61,95</sup>

Based on the theory of MOSFET, the drain current ( $I_D$ ) of the ISFET in the linear regime is given by:<sup>61,96–99</sup>

$$I_D = C_{OX}\mu \frac{W}{L} \left[ (V_{GS} - V_{TH})V_{DS} - \frac{1}{2}V_{DS}^2 \right] \quad (7)$$

where  $C_{OX}$  is the gate dielectric capacitance per unit area;  $\mu$  is the charge carrier mobility;  $W$  and  $L$  are the transistor's channel width and length, respectively;  $V_{GS}$  is the potential difference between gate and source electrode; and  $V_{TH}$  is the threshold voltage of the transistor. The threshold voltage can be further expressed as:<sup>61,96,97</sup>

$$V_{TH} = E_{ref} - \Psi + \chi^{sol} - \frac{\phi_{SC}}{q} - \frac{Q_{OX} + Q_{SS} + Q_B}{C_{OX}} + 2\phi_f \quad (8)$$

where  $E_{ref}$  is the potential of reference electrode;  $\Psi$  is the surface potential at the dielectric, which is a function of pH;  $\chi^{sol}$  is the surface dipole potential of the solution;  $\phi_{SC}$  is the work-function of semiconductor;  $q$  is the elementary charge;  $Q_{OX}$  is the accumulated charge per unit area in the dielectric;  $Q_{SS}$  is the accumulated charge per unit area at the dielectric–semiconductor interface;  $Q_B$  is the depletion charge per unit area in the semiconductor; and  $\phi_f$  is the Fermi voltage.

From the above two equations, one can see that the electrolyte–insulator–semiconductor (EIS) structure determines the threshold voltage and consequently the current–voltage behavior of the ISFET. A theory from site-dissociation and double-layer models was developed to express the surface potential ( $\Psi$ ):<sup>61,96,97</sup>

$$\Psi = 2.3 \frac{kT}{q} \frac{\beta}{\beta + 1} (\text{pH}_{pzc} - \text{pH}) \quad (9)$$

where  $k$  is the Boltzmann's constant;  $T$  is the absolute temperature;  $\beta$  is the acidic and basic equilibrium constants of the related surface reactions;  $\text{pH}_{pzc}$  is the pH value for which the dielectric surface is electrically neutral. Among these parameters,  $\beta$  represents the capability of chemical sensing of the oxide or dielectric. If  $\beta$  is large enough, we can assume  $\beta/(\beta + 1) = 1$ . In this case, at 25 °C, the change of 1 pH unit will result in the change of surface potential of 59.16 mV (also known as Nernst-response). In terms of pH sensors,  $\beta$  is related to the surface binding sites for  $\text{H}_3\text{O}^+$  (such as  $-\text{OH}$  groups) and is defined as:<sup>100</sup>

$$\beta = \frac{2q^2 N_s (K_b/K_a)^{1/2}}{kT C_{DL}} \quad (10)$$

where  $N_s$  is the total number of surface binding sites per unit area;  $K_a$  and  $K_b$  are the equilibrium constants of acid and base point, respectively;  $C_{DL}$  is the double-layer capacitance at the dielectric–electrolyte interface derived from the Gouy–Chapman–Stern model. As a result, if a gate dielectric has a significant amount of surface binding sites for  $\text{H}_3\text{O}^+$ , then the surface potential of the dielectric can be shifted by a measurable amplitude. For ISFETs, the variation of threshold voltage or drain current can be recorded to determine the pH variation. Furthermore, the thin-film transistor-based ISFET follows the same relation between surface potential and solution pH.

#### 3.2.2 Applicable materials and sensor performance: ISFET.

The sensing material in an ISFET should have extensive surface binding sites for  $\text{H}_3\text{O}^+$ . Most ISFETs, or EIS devices, were fabricated on doped silicon (Si) substrates. The insulation materials functioning as the pH-sensitive layer include metal oxides and semiconductor-based ceramics. Titanium oxide ( $\text{TiO}_2$ ) has been used in both EIS structures and ISFETs. The pH sensitivity of sputtered  $\text{TiO}_2$  film was around 57 mV per pH,<sup>101,102</sup> while the sensitivity was roughly 63 mV per pH for the  $\text{TiO}_2$  film prepared by metal–organic chemical vapor deposition (MOCVD).<sup>103</sup> The sensitivity of  $\text{TiO}_2$  is attributed to the hydrogen bonds formed at the oxide surface acting as binding sites. However, the formation of titanium hydroxide introduces large hysteresis during measurements. In addition, to get a densely-packed  $\text{TiO}_2$  layer, high-temperature annealing is required (normally above 500 °C).

Another attractive material for pH sensing is tantalum pentoxide ( $\text{Ta}_2\text{O}_5$ ). A near-Nernst response of about 57 mV per pH was obtained for this material prepared by MOCVD<sup>104</sup> or thermal oxidation.<sup>105</sup> The challenge of using  $\text{Ta}_2\text{O}_5$  is to avoid exposure to light. This is because light can generate charge carriers in  $\text{Ta}_2\text{O}_5$  and result in drift of the output signals. Other materials such as zinc oxide ( $\text{ZnO}$ ),<sup>106</sup> hafnium oxide ( $\text{HfO}_2$ ),<sup>107</sup> gadolinium oxide ( $\text{Gd}_2\text{O}_3$ ),<sup>108</sup> titanium-based binary oxides,<sup>109</sup> aluminum–gallium–nitride/gallium nitride ( $\text{AlGaIn/GaN}$ ),<sup>110</sup> and semiconductor nanowires<sup>111,112</sup> were used and they demonstrated with a sub-Nernst or near-Nernst pH responses.

Low-temperature (normally below 300 °C) deposition of the pH sensing layer is attractive for sensor development on polymeric substrate due to their low glass transition temperature.

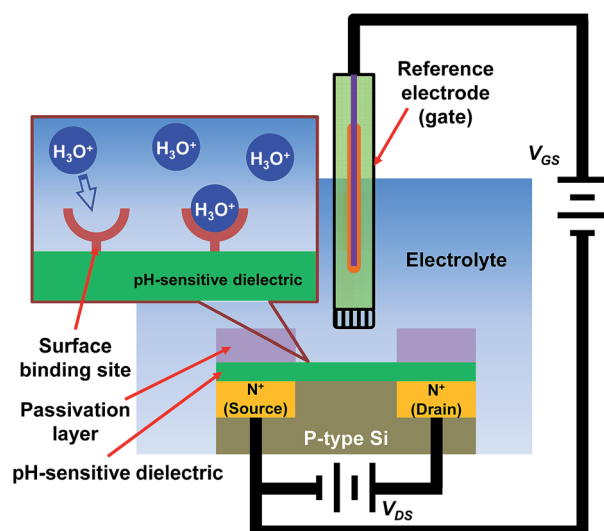


Fig. 3 Schematic of an ISFET-based pH sensor and its sensing mechanism.

Solution-processed aluminum oxide ( $\text{Al}_2\text{O}_3$ ) was spin coated onto graphene and annealed at  $250\text{ }^\circ\text{C}$ , offering a pH sensitivity of  $36.8\text{ mV per pH}$  in the pH range of 3 to 10.<sup>113</sup>  $\text{Ta}_2\text{O}_5$  layer was deposited onto graphene using atomic layer deposition (ALD) at low temperatures.<sup>114</sup> The pH sensing range of the graphene-based sensor is between 3 and 8 with a sensitivity of  $55\text{ mV per pH}$ .

Besides inorganic materials, organic semiconductors were also used for the channel in an ISFET. Poly(3-hexylthiophene) (P3HT) and pentacene were also used in ISFET-based pH sensors.<sup>115–118</sup> They can be integrated not only with metal oxide sensing layers, but also with organic thin films having hydrogen ionophores or  $\text{H}_3\text{O}^+$  binding sites. Polytriarylamine (PTAA) has superior electrical stability to other organic semiconductors. It was coated with the insulating material  $\text{Al}_2\text{O}_3$  (ref. 119 and 120) and polyisobutylmethacrylate–Teflon as a bi-layer. Depending on the insulating material, the pH sensitivity varied from  $33\text{ mV per pH}$  ( $\text{Al}_2\text{O}_3$ ) to over  $60\text{ mV per pH}$  (polyisobutylmethacrylate–Teflon). Importantly, PTAA enabled the stable operation of such sensors for more than 5000 cycles of measurement.<sup>119</sup> Due to the low mobility of organic semiconductors, the operation voltages of these sensors are higher (normally tens of volts) than that of Si-based ones.

**3.2.3 Sensor configuration and sensing mechanism: ExGFET.** The extended-gate field-effect transistor (ExGFET), invented in 1983, is a modified version of the ISFET.<sup>121</sup> An ExGFET is a MOSFET or thin film transistor with an extended gate electrode, in which a large part of the extended gate is away from the active area of the transistor, as shown in Fig. 4.

During sensing, only the extended-gate is immersed in the solution while the other parts stay dry. Because of its structure, the ExGFETs exhibit several advantages over traditional ISFETs:<sup>122</sup>

- (1) Lower cost since the pH sensing electrodes can be connected to the gate of commercialized MOSFETs (users do not have to fabricate their own transistors).
- (2) Easier packaging because the whole ExGFET is physically connected (without solution between gate and dielectric).
- (3) Better stability since the major part of the sensor can be used in dry environment.

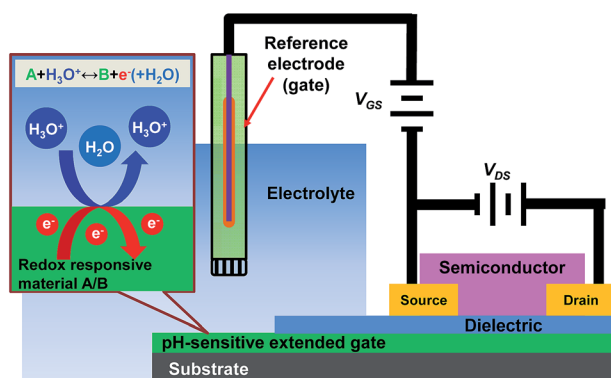


Fig. 4 Schematic of an ExGFET-based pH sensor and its sensing mechanism.

The major difference between ISFETs and ExGFETs is the impedance of the sensing films.<sup>123,124</sup> In an ISFET, the sensing layer is the gate dielectric, which has to be defect-free and of high-impedance. The sensing membrane in an ExGFET has to be low-impedance and  $\text{H}_3\text{O}^+$  changes the potential at the gate. The effective threshold voltage of an ExGFET when performing sensing can be written as:<sup>125</sup>

$$V_{t, \text{EXG}} = V_{\text{TH}} + E_{\text{ref}} - \psi + \chi^{\text{sol}} - \frac{\phi_{\text{M}}}{q} \quad (11)$$

where  $V_{\text{TH}}$  is the threshold voltage of the ExGFET when not performing sensing;  $\psi$  is the surface potential at the electrolyte–gate interface, which is a function of pH; and  $\phi_{\text{M}}$  is the work function of gate metal. Since the pH–surface potential relation for ExGFETs is identical to that for ISFETs, then different pH values will result in different threshold voltages and drain currents.

**3.2.4 Applicable materials and sensor performance: ExGFET.** In case of ExGFET, low-impedance sensing layers have to be used. In contrast to insulating  $\text{TiO}_2$  films in ISFETs, semiconductive  $\text{TiO}_2$  nanostructures were used in ExGFETs.  $\text{TiO}_2$  nanoparticles deposited by sol–gel methods exhibited pH responses between  $50$  and  $61\text{ mV per pH}$  in the pH range between 1 and 11.<sup>125–127</sup> However, significant hysteresis and drift were observed, which might be due to the nanoporous nature of the sensing films made from nanoparticles. Furthermore, such sensing films require high temperature ( $>500\text{ }^\circ\text{C}$ ) annealing as a post-treatment to achieve optimized performance.

To address the issue of high-temperature processing, hydrothermal growth of  $\text{TiO}_2$  nanowires<sup>128</sup> and nanorods<sup>129</sup> were performed at  $150\text{ }^\circ\text{C}$ . However, the processing time with this approach is much longer than that of other growth methods. Similarly,  $\text{ZnO}$  nanowalls<sup>122</sup> and nanowires<sup>130</sup> prepared by chemical bathing and ALD were sensitive to pH. But their response was poorer than  $\text{TiO}_2$ . Other metal oxides that were used in an ExGFET-based pH sensor include niobium pentoxide,<sup>131</sup>  $\text{PdO}$ ,<sup>132</sup> and tin oxide.<sup>133</sup> They were less widely studied due to either their relatively poor sensing performance, or the requirement for extreme fabrication conditions such as the use of high temperatures.

Organic–inorganic hybrid materials were studied to utilize the benefits from both types of materials. For instance, CNTs were used with indium oxide in a bi-layer and core–shell configurations.<sup>134,135</sup> CNTs and nickel have been plated together to form CNT–nickel oxide composite structure.<sup>136</sup> The metal oxides normally behave as the  $\text{H}_3\text{O}^+$  binder and CNTs are employed to regulate the conductivity of the film. Although these composite materials did not perform as well as metal oxides, the ease in adjusting material properties by varying processing steps and parameters are important advantages.

Pure organic materials are less frequently reported as the sensing component in an ExGFET. Parylene-C, one of the few examples, was treated with oxygen plasma to generate surface functional groups for  $\text{H}_3\text{O}^+$  binding.<sup>137</sup> The resulting pH sensitivity of  $23\text{ mV per pH}$  in the pH range of 4 to 10 was relatively low. This poor performance left room for more research work in this area.

### 3.3 Chemo-resistor/-transistor

**3.3.1 Sensor configuration and sensing mechanism: chemo-resistor.** A chemo-resistor-based pH sensor is a two-terminal device with the pH sensitive material deposited between two electrodes (Fig. 5). The sensing material has an intrinsic electrical resistance/conductance, which will change accordingly upon exposure to solutions with different pH values. The mechanisms for the change in resistance/conductance are the following.<sup>138</sup>

(1) The chemical reactions between  $\text{H}_3\text{O}^+$  or  $\text{OH}^-$  with the sensing material that generates new materials with different electrical properties.

(2) The  $\text{H}_3\text{O}^+$ -induced changes in the charge depletion/accumulation layer in the semiconductive sensing material.

The chemo-resistor has a simple physical structure and it does not require a reference electrode. These two features are preferred for miniaturization of the sensor.

**3.3.2 Applicable materials and sensor performance: chemo-resistor.** For chemo-resistors,  $\text{TiO}_2$  nanowires have been synthesized at the surface of Ti/Carbon nanofibers by electro-spinning and hydrothermal growth.<sup>139</sup> The high-concentration  $\text{H}_3\text{O}^+$  in the solution reduces the depletion layer at the surface of n-type  $\text{TiO}_2$  nanowires, thus increasing the electrical conductivity of the material. In the pH range between 2 and 12, such a sensor showed a response of 5.7 nS per pH. On the other hand, Pd is known as a hydrogen storage material owing to the formation of Pd-H hydride, which possesses an electrical resistivity 1.3 to 2 times higher than Pd.<sup>140</sup> Based on the resistivity change, Lee *et al.*<sup>140</sup> used standard photolithography to fabricate Pd resistors and gold (Au) electrodes. Hydrogen gas generated during electrolysis was sensed by the Pd resistor and its resistance was proportional to the concentration of  $\text{H}_3\text{O}^+$  in the solution (higher concentration generated more hydrogen gas). A change of 1 unit pH caused the Pd resistance to vary 5% from its initial value.

Graphene and CNTs were also studied in chemo-resistors.<sup>138,141</sup> Their pH sensing mechanism can be attributed to the

adsorption of  $\text{H}_3\text{O}^+$  and  $\text{OH}^-$  at their surface sites. The adsorbed ions make the carbon nanomaterials doped or de-doped, resulting in the variation of resistance. Annealed graphene had a pH sensitivity of 2000  $\Omega$  per pH between pH of 4 and 10, while the value was 65  $\Omega$  per pH in the pH range from 5 to 9 for multi-wall CNTs. Note that it is more meaningful to compare the response using resistivity rather than resistance. However, the resistivity values were not reported in these articles.

**3.3.3 Sensor configuration and sensing mechanism: ECT.** Sometimes, the pH sensing material is not easily affected by the  $\text{H}_3\text{O}^+$ , so sensitivity is low. Therefore, an extra electrode can be incorporated into the chemo-resistor to form a chemo-transistor. The extra electrode is the gate of the chemo-transistor and its functions to modulate the output current.<sup>142</sup> If the gate electrode is separated from the transistor and placed in the solution, then the device could be an electrochemical transistor (ECT, Fig. 6).

In contrast to an ISFET, there is no oxide/dielectric layer between the semiconductor and solution.<sup>38</sup> The conductivity of the channel is controlled by the electrochemical doping/de-doping process at the semiconductor-solution interface. The doping/de-doping process comprises reversible transportation of mobile ions into/out of the semiconductor. Also, the channel can be switched between different doping levels by the gate bias.<sup>40</sup> Organic semiconductors are the preferred materials in ECTs because the modification of their electrical properties is relative easier when compared to inorganic ones. When there is no gate voltage applied, the output current is determined by the intrinsic conductance of the organic semiconductor (assume it is p-type).<sup>143</sup> If the gate voltage is positive, the  $\text{H}_3\text{O}^+$  (can be other cations) in the solution will be pushed into the semiconductor by the electrical field to dope the material, which increases the charge carrier density in the channel. Consequently, the output current will increase. However, reversibility of the sensor is poor, which is attributed to the electrochemical-process-induced material degradation.

**3.3.4 Applicable materials and sensor performance: ECT.** ECT-based pH sensors generally use organic materials as the

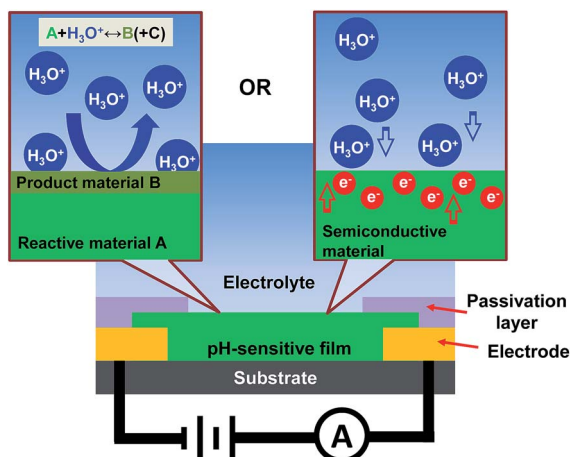


Fig. 5 Schematic of a pH sensor in chemo-resistor structure and its possible sensing mechanisms.

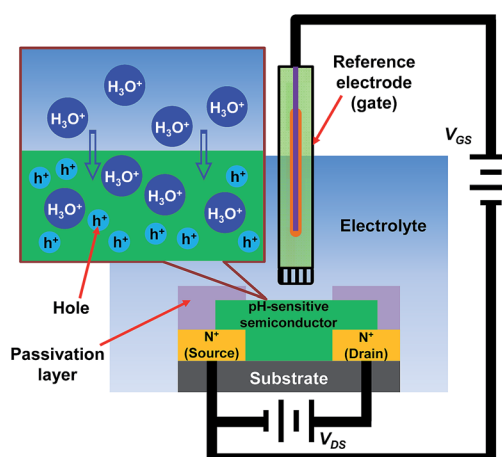


Fig. 6 Schematic of an ECT-based pH sensor and its sensing mechanism.

channel and sensing layer. The influence of  $\text{H}_3\text{O}^+$  on charge transport in the P3HT channel in an ECT was observed. The output current had a 10 nA per pH response when the pH was varied between 4 and 10.<sup>144</sup> However, due to the electrochemical reaction of the sensing material, the lifetime of this ECT-based sensor was short, around 12 hours. To improve the lifetime of the sensor by reducing material degradation and delamination, AC measurement can be used.

Poly(3,4-ethylenedioxythiophene) doped with polystyrene sulfonate (PEDOT:PSS) is a conductive polymer whose conductivity can be tuned by the extra doping of  $\text{H}_3\text{O}^+$ .<sup>145</sup> The injection of  $\text{H}_3\text{O}^+$  could turn highly conductive PEDOT<sup>+</sup> to less conductive PEDOT<sup>0</sup>. Thus, in order to get the identical output current, the effective gate voltage had to be increased. A pH sensitivity of 64.2 mV per pH was realized. Since reliability is of great concern for ECT-based sensors, Gou *et al.* oxidized single-walled CNTs and functionalized them with poly(1-aminoanthracene) (PAA) to prepare the pH sensing material.<sup>62</sup> The response of the sensor was 73 mS per pH and demonstrated a wide pH sensing range between pH = 2 and 12. Also, very importantly, this sensor had a long lifetime of over 120 days.

**3.3.5 Sensor configuration and sensing mechanism: EGFET.** An electrolyte-gated field-effect transistor (EGFET) has the identical physical structure of an ECT. It consists of the semiconductor which does not react with the solution. Instead, an electrical double layer (EDL, or Debye–Helmholtz double layer) at the electrolyte–semiconductor interface is formed.<sup>143,146</sup> In a p-channel EGFET (Fig. 7), if the gate voltage is negative, the anions in the solution migrate to the semiconductor–solution interface while the cations travel to the solution–gate interface, resulting in the formation of EDLs. According to the Gouy–Chapman–Stern model, the EDL consists of excess electrons (or holes) along the metal gate (semiconductor) surface, and a layer of cations (anions) at the electrolyte side. The cations (anions) layer is composed of two layers, the compact layer (or Helmholtz layer, HL) and the diffusion layer.<sup>147</sup> Because ions are solvated in the solution, the HL is composed of a single layer of solvent molecules and a single layer of solvated ions.<sup>148</sup> The diffusion layer consists of free cations (anions) driven by the electrostatic interaction and thermal motion. The concentration of cations (anions) decreases with the distance from the gate (semiconductor). The electrical potential drops at the gate (semiconductor)–solution interface in the EDLs, which is an analogue of a capacitor. The capacitance of the EDL ( $C_d$ ) can be expressed as:<sup>147</sup>

$$\frac{1}{C_d} = \frac{x}{\epsilon} + \frac{1}{\left(\frac{2\epsilon n^2 e^2 \alpha}{kT}\right)^{\frac{1}{2}} \cosh\left(\frac{nq\phi}{2kT}\right)} \quad (12)$$

In eqn (12),  $x$  is the thickness of the HL,  $\epsilon$  is the permittivity of the HL,  $\alpha$  is the ion concentration in the bulk solution,  $n$  is the charge on the ion, and  $\phi$  is the electrical potential at the HL–diffusion layer interface, which is also the plane having a distance  $x$  to the gate (semiconductor). This distance  $x$  is also a function of the ion concentration in the bulk solution:

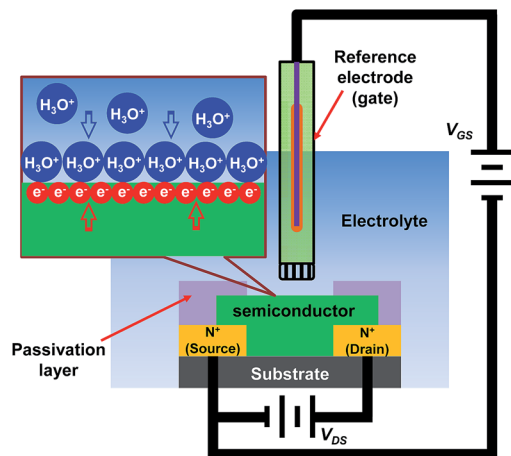


Fig. 7 Schematic of an EGFET-based pH sensor and its sensing mechanism.

$$x = \frac{3.3 \times 10^6 \epsilon}{z\alpha^{\frac{1}{2}}} \quad (13)$$

Because the thickness of the EDL is extremely small (typically less than 0.1 Å in metals and 10 Å in solutions), the capacitance can be as high as a few to hundreds of  $\mu\text{F cm}^{-2}$  (typical values are between 10  $\mu\text{F cm}^{-2}$  and 500  $\mu\text{F cm}^{-2}$ , compared to 10 nF  $\text{cm}^{-2}$  for 300 nm thick silicon dioxide),<sup>143</sup> which enables low operation voltage of the transistor. The pH sensitivity is determined by the gate capacitance as a function of  $\text{H}_3\text{O}^+$  concentration. When pH increases,  $\alpha$  decreases,  $x$  increases,  $C_d$  decreases, and the output current decreases. The disadvantages of EGFET-based sensors include their long response time due to the construction of the EDL, the difficulty in sensing high-concentration solutions (such as a solution of pH = 1), as well as the poor selectivity of ions.

**3.3.6 Applicable materials and sensor performance: EGFET.** Using an EGFET, a pH response was observed in the output current when the solution pH is between 7 and 9.<sup>149</sup> In such a device, ZnO nanowires were decorated by Pd or Au nanoparticles, which induced quasi-spherical charge depletion regions in the 1D (nanowire) transport channel. However, important performance parameters such as sensitivity were not reported. Graphene, CNTs, and P3HT, deposited by low-temperature technologies were characterized in EGFET-based pH sensors.<sup>150–152</sup> They displayed low sensitivities around 28 mV per pH, which may be due to the instability of the materials in an aqueous environment. However, Ang *et al.* grew a few-layer graphene film at 1100 °C and manually mounted the sensing layer to an EGFET.<sup>153</sup> A sensitivity of about 100 mV per pH was achieved in the pH range from 2 to 12. This high sensitivity indicated the combined effect of surface potential modulation and ion adsorption.

**3.3.7 Sensor configuration and sensing mechanism: FET.** The ECT- and EGFET-based sensors discussed above are not preferred for miniaturized devices due to the floating gate. An alternative way to reduce the dimensions of the device is to fabricate the gate beneath the semiconductor and dielectric, the same as a bottom-gate thin-film transistor (Fig. 8).<sup>142</sup> In such

FET-based sensor, three mechanisms were used to explain the sensing behavior.<sup>142</sup>

(1) The direct interaction between the semiconductor and ions (for example, charge transfer and doping/de-doping can alter the conductivity of semiconductor).

(2) The adsorption and diffusion of ions along the grain boundaries in the semiconductor, which may create deep-energy traps and increase the resistance of inter-grain charge transport.

(3) The local screening of the electrical field, due to the accumulation of ions at the semiconductor–solution interface.

During operation, the gate bias and the source–drain bias are set to generate a current flow through the channel.<sup>154</sup> The presence of  $\text{H}_3\text{O}^+$  adsorption or interaction is subsequently transduced to a change in the source–drain current. To make the sensing process reversible, an opposite polarity bias can be applied to the gate to desorb the weakly bonded ions.<sup>155</sup> The challenges for FET-based sensors are the high operating voltage, the drift of output current induced by gate-bias stress, and the stability of the sensing material in an aqueous environment.<sup>156–158</sup>

### 3.3.8 Applicable materials and sensor performance: FET.

For FET-based sensors, Ahn *et al.* introduced a dual-gate transistor with Si nanowires as the channel on a silicon-on-insulator platform.<sup>159</sup> These sensors had a sensitivity of 68 mV per pH, but the drift rate of 27 mV per hour made it unsuitable for long-term monitoring. Instead, some organic materials with a high stability in water were developed.<sup>157,160</sup> For example, 5,5-bis-(7-dodecyl-9H-fluoren-2-yl)-2,2-bithiophene was synthesized as a p-type semiconductor that can trap diffused  $\text{H}_3\text{O}^+$  in the grain boundaries.<sup>160</sup> The output current of the FET responded to the change of pH value at 50 nA per pH over  $10^4$  measurement cycles.

## 3.4 Challenges in developing microfabricated electrochemical pH sensor

Although many microfabricated electrochemical pH sensors have been reported, several challenges remain. One challenge is

related to the performance of the sensors. For sensors with sub-Nernst response, studies should focus on improving sensitivity. Many sensors exhibited near-Nernst or super-Nernst response. For these sensors, their stability and repeatability become the major concern. The instability and poor repeatability in long-term use most likely originate from the following phenomena.

**3.4.1 Degradation of sensing materials.** The degradation can be either physical or chemical. Physical degradation indicates that the sensing material at the sensor surface mechanically leaves the substrate and enters the solution. This is likely to happen in a pH sensor in online water quality monitoring system since the flow rate of water is typically fast and it can physically impact the sensor surface. This physical process influences the sensitivity by exposing the underlying material which may not be as sensitive as the surface material. Also, the surface of the sensing area may become rougher and result in a longer response time. Moreover, voids and pinholes may be generated in the sensing film, reducing the mechanical stability and reliability of the sensor.

Chemical degradation happens when irreversible reaction(s) happens between the sensing material and  $\text{H}_3\text{O}^+$ , or when the redox reaction is not fully reversible. In water quality monitoring systems, treated water contains residual chlorine, which is a strong oxidizing reagent for many organic materials. These reactions alter the chemical composition of the sensing material which affects sensitivity, and also may introduce slow-reaction sites which results in increased hysteresis. Both physical and chemical degradation can result in increases in the drift rate of the sensor since the properties of sensor surface keep changing with time. Thus, new sensing materials with better physical and chemical stability (except for the reversible reactions with  $\text{H}_3\text{O}^+$ ) have to be developed.

**3.4.2 Interference from the test solution.** The interference can originate from the adsorption of other ions or from bio-fouling. pH sensors based on ISFETs, ECTs, EGFETs, and FETs are more prone to alkaline ions since they can be adsorbed on pH sensing surfaces. The interfering ions introduce an electrical field to the channel of the transistor, thus affecting its output electrical characteristics. Bio-fouling commonly happens in water quality monitoring devices. The fouling layer may deteriorate the functionality of sensors by blocking the redox reaction between the sensing material and  $\text{H}_3\text{O}^+$ , or by preventing the adsorption of  $\text{H}_3\text{O}^+$  onto the sensor surface. To reduce interference from the solution, an ion-selective membrane and an anti-fouling coating should be applied to the surface of the sensors.

**3.4.3 Instability of the electronic components.** This mostly happens in pH sensors using transistor configurations with organic semiconductors. The electrical properties of organic semiconductors change with time, which is less stable than conventionally used silicon. As a consequence of the non-predictable behavior of the organic semiconductor, the repeatability of the pH sensor will be poor. Therefore, more research in the area of organic electronics is needed to obtain stable and reliable device performance using improved organic materials.

Another challenge is related to the microfabrication technologies. The cost of the sensors for water quality monitoring

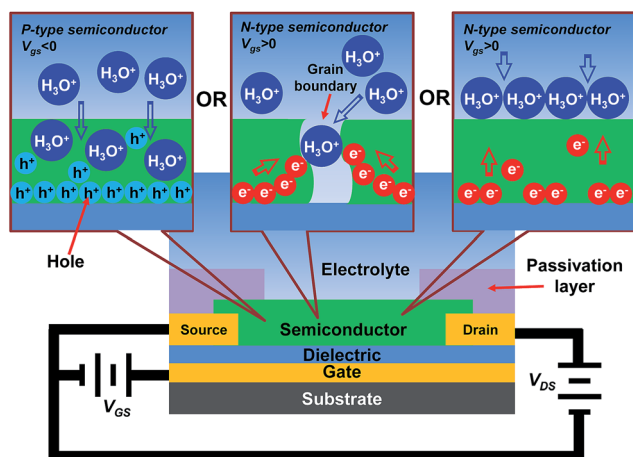


Fig. 8 Schematic of a pH sensor in FET structure and its possible sensing mechanisms.

should not be high. This requires the fabrication to be cheap and use small amount of materials. Also, process conditions at high temperatures and in vacuum environment should be avoided. Solution-based low-cost and large-area processing is potentially promising, but the quality of deposited materials is problematic (usually high-temperature treatment should be done after solution processing for a high-performance sensor). Therefore, there is a tradeoff between performance and cost of sensors. High-quality sensing materials that can be deposited using cost-effective ways are desired.

### 3.5 Summary for microfabricated electrochemical pH sensor

Microfabricated pH sensors based on potentiometric electrodes, ISFETs, and chemo-resistor/transistors have been reviewed in terms of their physical configurations and sensing mechanisms. The physical structures of the pH sensors are determined by the electrical properties (such as conductivity) and chemical features (such as solubility in water and chemical reactivity) of the sensing materials. The widely studied sensing materials include metal oxides, ceramics, polymers, and carbon nanomaterials. The sensing performance of microfabricated electrochemical pH sensors varies a lot (for example, from sub-Nernst response to super-Nernst response). This variation could be attributed to the intrinsic properties of the materials and their properties after processing. Therefore, the physical design, material selection, and microfabrication conditions are three key factors in the quest for low-cost, highly sensitive, fast-response and easy-to-use pH sensors.

The conventional glass pH electrode is compared with different types of microfabricated electrochemical pH sensors (Table 1). In Table 2, a listing of recent microfabricated electrochemical pH sensors is provided. The list includes sensor structures, sensing materials, key performance parameters, and corresponding fabrication processes. It has been observed that the size and cost disadvantages of the glass electrodes stimulated research in microfabrication of different kinds of electrochemical pH sensors. However, further research is needed to develop new materials and microfabrication processes, as well as to optimize their compatibility for low-cost and high-performance pH sensors.

## 4 Microfabricated electrochemical free chlorine sensors

As discussed in Section 1, two most commonly used approaches for free chlorine detection are DPD-based colorimetric and amperometric-based electrochemical methods. However, their large footprint limits their application in online water quality monitoring. Banna *et al.* briefly reviewed the miniaturized chlorine sensors,<sup>11</sup> focusing on microwire-based amperometric sensors and interferometry sensors. In this section, electrochemical free chlorine sensors having planar structures are reviewed due to their potential of miniaturization and integration with microelectronic devices.

### 4.1 Amperometric sensor configuration and sensing mechanism

Amperometric sensing is based on the voltammetric sensing method, which requires three electrodes: working, counter, and reference, for precise measurement.<sup>67</sup> A time-dependent electrical potential is applied to the working electrode, while the current flowing between the working and counter electrodes is measured (Fig. 9). The reference electrode is used to provide a fixed potential of the electrolyte. The potential sweep from a small to a large value can generate a current peak if the analyte is oxidized in that potential range. The creation of the peak is due to the oxidation of the analyte while the decline of the peak is because of the depletion of the analyte at the electrode surface. Conversely, when the potential sweeps from high to low, a reduction peak will be generated.

In amperometric sensing, a constant potential is applied between the working and reference electrodes and the current is monitored between the working and counter electrodes.<sup>67</sup> The constant potential is determined based on the position of redox peaks in the corresponding voltammetric waveform. At the selected potential, the redox reaction of the analyte should take place, and the interference of other ions should be avoided. The amplitude of measured current is proportional to the analyte concentration in the solution.

In an amperometric free chlorine sensor, the working electrode is normally made of noble metals such as gold (Au) and platinum (Pt), and is sometimes coated with a selective membrane for chlorine ions. At the working electrode, free chlorine is electrochemically reduced by applying a constant potential *versus* the reference electrode.<sup>161</sup> For example, at pH = 5.5, the reduction peak of HOCl and/or OCl<sup>-</sup> was observed at +0.4 V on a Au electrode with respect to a Ag/AgCl reference electrode. The electrochemical reactions at the working electrode can be written as the following equations.



The transfer of electrons generates a current which is proportional to the free chlorine concentration. Note that the pH, temperature, flow rate and pressure of the solution must be carefully controlled for an accurate measurement.

### 4.2 Applicable materials and sensor performance

A limited range of electrode materials using microfabrication technologies has been demonstrated to create miniaturized free chlorine sensors. For example, Au working and counter electrodes were deposited by electron-beam evaporation on cyclic olefin copolymer, where the Ag/AgCl reference electrode was electrochemically deposited.<sup>162</sup> Both electrodes were capped by microfluidic channels through which the analyte flowed. This low-cost and disposable sensor was operated under 0.1 V bias, and had a linear detection range of OCl<sup>-</sup> from 1.5 to 8 ppm. The current density in the counter electrode showed a sensitivity of about 69  $\mu\text{A cm}^{-2}$  per ppm. The lifetime of this sensor was

Table 1 Comparison of glass pH electrodes and different types of microfabricated electrochemical pH sensors

	Advantages	Disadvantages
Glass electrode	<ol style="list-style-type: none"> <li>(1) Wide application temperature (from <math>&lt;0^{\circ}\text{C}</math> to <math>&gt;100^{\circ}\text{C}</math>)</li> <li>(2) Ideal Nernst response independent of redox interferences</li> <li>(3) High accuracy and resolution (0.001 pH unit)</li> <li>(4) High stability and long lifetime (several years)</li> </ol>	<ol style="list-style-type: none"> <li>(1) Unstable in strong alkaline and hydrofluoric acid solutions</li> <li>(2) Large in size</li> <li>(3) Brittle</li> <li>(4) Require frequent maintenance and calibration</li> <li>(5) Expensive</li> </ol>
Microfabricated electrochemical pH sensor	<ol style="list-style-type: none"> <li>(1) Small size</li> <li>(2) Easy for integration</li> <li>(3) Can be stored in dry condition</li> <li>(4) Low cost</li> <li>(5) Less frequent maintenance</li> </ol>	<ol style="list-style-type: none"> <li>(1) Low accuracy and resolution</li> <li>(2) Large hysteresis and drift</li> <li>(3) Poor ion selectivity</li> <li>(4) Sometimes sensitive to light</li> <li>(5) Limited application temperature</li> <li>(6) Require water-stable sensing material</li> </ol>
General	<ol style="list-style-type: none"> <li>(1) Simple structure</li> <li>(2) Power supply not needed</li> </ol>	<ol style="list-style-type: none"> <li>(1) Require reference electrode</li> <li>(2) No internal signal amplification</li> </ol>
Potentiometric electrode	<ol style="list-style-type: none"> <li>(1) Semiconductor protected by dielectric</li> <li>(2) Compatible with CMOS fabrication process</li> </ol>	<ol style="list-style-type: none"> <li>(1) Require reference electrode</li> <li>(2) Dielectric surface difficult to be functionalized for higher selectivity</li> </ol>
ISFET	<ol style="list-style-type: none"> <li>(1) Transistor can be used in dry condition</li> <li>(2) Compatible with CMOS fabrication process</li> <li>(3) Internal signal amplification</li> </ol>	<ol style="list-style-type: none"> <li>(1) Require reference electrode</li> <li>(2) Larger size due to extended gate</li> </ol>
EXGFET	<ol style="list-style-type: none"> <li>(1) Simple structure</li> <li>(2) Reference electrode not needed</li> </ol>	<ol style="list-style-type: none"> <li>(1) Low reversibility</li> <li>(2) Poor selectivity</li> </ol>
Chemo-resistor	<ol style="list-style-type: none"> <li>(1) Dielectric not needed</li> <li>(2) Low operation voltage</li> <li>(3) Higher sensitivity comparing to chemo-resistor</li> </ol>	<ol style="list-style-type: none"> <li>(3) Lower sensitivity comparing to ECT</li> <li>(4) No internal signal amplification</li> </ol>
ECT	<ol style="list-style-type: none"> <li>(1) Internal signal amplification</li> <li>(2) Dielectric not needed</li> <li>(3) Low operation voltage</li> </ol>	<ol style="list-style-type: none"> <li>(1) Require reference electrode</li> <li>(2) Low reversibility</li> <li>(3) Poor selectivity</li> </ol>
EGFET	<ol style="list-style-type: none"> <li>(3) Internal signal amplification</li> </ol>	<ol style="list-style-type: none"> <li>(4) Difficult in integration</li> <li>(1) Require reference electrode</li> <li>(2) Sensing is difficult in high-concentration electrolyte</li> </ol>
FET	<ol style="list-style-type: none"> <li>(1) Compact structure</li> <li>(2) Easy for integration</li> <li>(3) Reference electrode not needed</li> <li>(4) Internal signal amplification</li> </ol>	<ol style="list-style-type: none"> <li>(3) Low switching speed</li> <li>(4) Poor selectivity</li> <li>(1) Require water-stable semiconductors</li> <li>(2) High operation voltage</li> <li>(3) Large hysteresis</li> <li>(4) Low reversibility</li> </ol>

Table 2 Summary of microfabricated electrochemical pH sensors

Structure	Sensing material	Operation voltage [V]	Detection range [pH unit]	Sensitivity	Response time [s]	Stability	Fabrication of sensing materials	Ref.
Potentiometric	CuO	—	2–11	28 mV per pH	25	Drift = 150 mV h <sup>-1</sup>	Hydrothermal deposition	77
	IrO <sub>x</sub>	—	2–10	74 mV per pH	<100	Sensitivity reduces to 65 mV per pH in 14 days	Electrochemical deposition of IrO <sub>x</sub> in anodized Al <sub>2</sub> O <sub>3</sub>	74
	IrO <sub>x</sub>	—	2.38–11.61	69 mV per pH	<2	Potential variation <10 mV	Electrochemical deposition, annealing at >300 °C	73
	IrO <sub>x</sub>	—	4–9	70 mV per pH	—	—	Electrochemical deposition	72
	IrO <sub>2</sub>	—	1.56–12	74 mV per pH	—	Stable >7 days	Electrochemical deposition	187
	IrO <sub>2</sub>	—	1–13	59 mV per pH	<1	Drift <0.1 mV per day	Thermal oxidation at 870 °C	71
	IrO <sub>2</sub> + PMMA	—	3–11	60 mV per pH	<2	Stable >1 month	Hydrolysis of (NH <sub>4</sub> ) <sub>2</sub> IrCl <sub>6</sub> for IrO <sub>2</sub> , thermal molding with PMMA at 150 °C	76
	Ta <sub>2</sub> O <sub>5</sub> –IrO <sub>2</sub> bi-layer	—	2–13	60 mV per pH	15	Drift <0.1 mV h <sup>-1</sup>	RF sputtering	75
	S-Modified-α-Fe <sub>2</sub> O <sub>3</sub>	—	1.5–12.5	59 mV per pH	10	Stable <1 week	Hydrothermal synthesis, annealing at 600 °C	174
	Co <sub>3</sub> O <sub>4</sub>	—	3–13	58 mV per pH	53	Stable for 3 days	Hydrothermal deposition, annealing at 450 °C	78
	WO <sub>3</sub>	—	5–9	57 mV per pH	25	11.6% sensitivity decrease between 1 <sup>st</sup> and 3 <sup>rd</sup> measurement	Hydrothermal deposition	79
	WO <sub>3</sub>	—	2–12	55 mV per pH	—	Drift = 6 mV h <sup>-1</sup> ; 50 mV hysteresis	RF sputtering and O <sub>2</sub> plasma oxidation	188
	RuO <sub>2</sub>	—	1–13	57 mV per pH	—	—	RF sputtering	183
	RuO <sub>2</sub>	—	4–10	69 mV per pH	10	Potential fluctuation = 9 mV	RF sputtering	80
	TiO <sub>2</sub>	—	2–12	59 mV per pH	<30	—	Anodization, annealing at 450 °C	189
	ZnO	—	4–11	52 mV per pH	—	—	Hydrothermal deposition	190
	PbO <sub>2</sub>	—	0.25–13	84 mV per pH	—	—	Electrochemical deposition + electrochemical oxidation for 24 h	81
	Uric acid composite	—	4–10	73 mV per pH	—	—	Electrochemical deposition	191
	Diamond	—	2–12	51 mV per pH	<1	—	Hot filament CVD	192
	PANI	—	2–9	62 mV per pH	—	—	Electropolymerisation	83
	PANI	—	3–7	54 mV per pH	<25	Stable for 30 min on human body	Electropolymerisation	86
	PANI	—	2.69–8.51	59 mV per pH	<20	Stable >35 days	Electropolymerisation	87
	PANI	—	2–10	71 mV per pH	—	Stable for 5 weeks	Electropolymerisation	179
	PANI + CNT	—	1–13	58 mV per pH	<40	Drift between 2 and 10 mV h <sup>-1</sup>	Spray of GNT suspension, electrochemical deposition of PANI	193
	PANI:tetra-phenylborate	—	3–9	86 mV per pH	—	—	Electropolymerisation	194
	Parlylene C	—	4–10	16 mV per pH	—	Drift between 3 and 20 mV h <sup>-1</sup>	CVD + O <sub>2</sub> plasma etching	89
	PEI	—	2–11	46 mV per pH	15	Sensitivity decreases at 0.65 mV per pH day	Electropolymerisation	84
	Polybisphenol A	—	–1 to 15	57 mV per pH	<20	Stable >12 days	Electropolymerisation	195
	PEDOT:PSS	—	5.9–8.7	52 mV per pH	15	—	Electropolymerisation	196

Table 2 (Contd.)

Structure	Sensing material	Operation voltage [V]	Detection range [pH unit]	Sensitivity	Response time [s]	Stability	Fabrication of sensing materials	Ref.
EIS	PPY	—	2–11	51 mV per pH	120	3.2 mV per pH variation in sensitivity for 50 days	Electropolymerisation	85
	PPY: hydroquinone monosulfonate	—	2–12	51 mV per pH	<100	Stable for 30 days	Electropolymerisation	88
	CNT	—	3–11	60 mV per pH	<30	—	CNT deposited from solution	94
	Er <sub>2</sub> TiO <sub>5</sub>	3	2–12	57 mV per pH	—	Drift = 0.29 mV h <sup>-1</sup>	Reactive sputtering, rapid thermal annealing at 900 °C	109
	Gd <sub>2</sub> O <sub>3</sub>	2	2–10	55 mV per pH	—	Sensitivity decreases by 0.65 mV per pH in 12 h	Reactive sputtering, rapid thermal annealing at 800 °C	108
	Gd <sub>2</sub> Ti <sub>2</sub> O <sub>7</sub>	3	2–12	58 mV per pH	—	Drift = 0.38 mV h <sup>-1</sup>	Reactive sputtering, rapid thermal annealing at 900 °C	109
	Lu <sub>2</sub> Ti <sub>2</sub> O <sub>7</sub>	3	2–12	59 mV per pH	—	Drift = 0.55 mV h <sup>-1</sup>	Reactive sputtering, rapid thermal annealing at 900 °C	109
	Ta <sub>2</sub> O <sub>5</sub>	—	1–10	56 mV per pH	60	Drift = 5 mV h <sup>-1</sup>	Thermal oxidation at 525 °C	105
	TiO <sub>2</sub>	—	3–11	62 mV per pH	—	Drift = 0.9 mV per day	MOCVD, annealing at 700 to 900 °C	103
	NbO <sub>x</sub>	2.5	2–12	60 mV per pH	—	Drift = 3 mV h <sup>-1</sup>	RF sputtering, rapid thermal annealing at 700 °C	197
ISFET	InAs	0.9	4.7–7.8	48 mV per pH	—	—	Molecular beam epitaxy	112
	AlGaN/GaN	10	4–9	52 mV per pH	—	—	ICP etching, annealing at 850 °C	110
	Ga <sub>x</sub> O <sub>y</sub>	1.5	2–12	55 mV per pH	—	Drift = 1.41 μA h <sup>-1</sup> ; hysteresis = 0.4 mV; sensitivity decreases at 0.14 mV per pH per day	MOCVD, rapid thermal annealing at 900 °C, H <sub>2</sub> O <sub>2</sub> surface treatment	198
	HfO <sub>2</sub>	2	3–10	60 mV per pH	—	—	ALD, annealing at 450 °C	107
	HfO <sub>2</sub>	8	3–10	57 mV per pH	120	Drift = 0.1 mV h <sup>-1</sup> at pH = 6; hysteresis = 8 mV	Electron-beam lithography, thermal SiO <sub>2</sub> growth, ALD of HfO <sub>2</sub>	199
	SiO <sub>2</sub>	6	3–12	363 mV per pH	—	Drift = 3 mV h <sup>-1</sup> ; hysteresis = 13 mV	RF sputtering, rapid thermal annealing at 450 °C	173
	SiO <sub>2</sub>	3	4–10	168 mV per pH	—	—	PECVD	175
	TiO <sub>2</sub>	4	1–13	57 mV per pH	—	—	RF sputtering, annealing at 500 °C	101 and 102
	Ta <sub>2</sub> O <sub>5</sub>	1.2	3–8	55 mV per pH	—	Drift = 1 mV per week	ALD	114
	Ta <sub>2</sub> O <sub>5</sub>	12	3–8	120 mV per pH	—	—	RF sputtering, annealing at 300 °C	174
Graphene + Al <sub>2</sub> O <sub>3</sub>	Yb <sub>2</sub> O <sub>3</sub>	2	2–12	56 mV per pH	60	Drift = 1.54 mV h <sup>-1</sup>	Reactive sputtering, rapid thermal annealing at 800 °C	200
	ZnO	3	2–12	42 mV per pH	—	Drift = 1.78 mV h <sup>-1</sup>	RF sputtering, annealing at >600 °C	106
	Graphene + Al <sub>2</sub> O <sub>3</sub>	60	3–10	37 mV per pH	200	Drift = 6.34 mV h <sup>-1</sup>	Rapid thermal CVD of graphene at 950 °C + low temperature transferring; spin coating of Al <sub>2</sub> O <sub>3</sub> + annealing at 250 °C	113

Table 2 (Contd.)

Structure	Sensing material	Operation voltage [V]	Detection range [pH unit]	Sensitivity	Response time [s]	Stability	Fabrication of sensing materials	Ref.
	P3HT + valinomycin membrane	1	3.4–5.6	3 nA per pH	360	—	P3HT spin coating, valinomycin membrane deposited by Langmuir–Blodgett technique	115
	P3HT + Ta <sub>2</sub> O <sub>5</sub> + valinomycin membrane	5	6.6–9.5	71 nA per pH	—	—	RF sputtering of Ta <sub>2</sub> O <sub>5</sub> , solution casting of valinomycin membrane, P3HT spin coating	201
	P3HT + arachidic acid	1	3.3–5.5	4 nA per pH	100	—	Spin coating of P3HT, arachidic acid deposited by Langmuir–Blodgett technique	116
	P3HT + multi-layer hydrogen inopore	0.6	3–12	25–52 mV per pH	—	Stable for 30 s	Drop casting of PVC, 2-NPOE, NaTFPB, and hydrogen inopore	117
	Pentacene	100	4–10	30 nA per pH	>2000	—	Pentacene: vacuum sublimination.	118
	Pentacene/PTAA + Al <sub>2</sub> O <sub>3</sub>	4	2–12	5 nA per pH	30	Stable for >5000 cycles	TIPS-pentacene spin coating, ALD of Al <sub>2</sub> O <sub>3</sub>	119
	PTAA + PIBMA + Teflon	40	2–10	60 mV per pH	—	—	PTAA spin coating, Teflon spin coating	120
ExGFET	Nb <sub>2</sub> O <sub>5</sub>	6	2–12	52 mV per pH	75	Drift = 3.34 mV h <sup>-1</sup>	RF sputtering + CF <sub>4</sub> plasma treatment, rapid thermal annealing at 600 °C	131
	TiO <sub>2</sub> :Ru	6	1–13	55 mV per pH	—	Drift = 0.745 mV h <sup>-1</sup>	RF sputtering of TiO <sub>2</sub> , DC sputtering of Ru, annealing at 600 °C	123
	TiO <sub>2</sub>	6	1–11	59 mV per pH	40	Drift = 1.97 mV h <sup>-1</sup>	Sol-gel spin coating, annealing at 600 °C	127
	TiO <sub>2</sub>	5	2–12	50 mV per pH	—	—	Hydrothermal deposition	129
	TiO <sub>2</sub>	5	2–12	62 mV per pH	—	—	Hydrothermal deposition	128
	TiO <sub>2</sub>	10	1–11	61 mV per pH	—	Drift between 9 and 60 mV h <sup>-1</sup>	Sol-gel spin coating, annealing <500 °C	125
	TiO <sub>2</sub> -PPI bi-layer	—	4–10	57 mV per pH	—	—	Layer-by-layer deposition of PPI and TiO <sub>2</sub> from solution	126
	In <sub>2</sub> O <sub>3</sub> -CNT bi-layer	3	2–12	36 mV per pH	—	—	Sputtering of In, spray coating of CNTs, annealing at 400 °C	134 and 135
	SnO <sub>2</sub>	40	3–10	287 mV per pH	—	Drift = 48.77 mV h <sup>-1</sup>	RF sputtering, microwave annealing at 1000 W (~87 °C)	172
	SnO <sub>2</sub> :F	5	2–12	50 mV per pH	—	—	Vacuum deposition	133
	PdO	2	2–12	63 mV per pH	—	Drift = 2.32 mV h <sup>-1</sup> ; hysteresis = 7.9 mV; stable for 6 measurement cycles	Reactive e-beam evaporation + annealing at 700 °C	132
	ZnO	6	2–12	38 mV per pH	—	—	Sol-gel brushing, annealing at 150 °C	100
	ZnO	10	1–9	59 mV per pH	—	—	Hydrothermal deposition	122
	ZnO	6	5–9	18 mV per pH	—	—	Hydrothermal deposition	202
	ZnO	4	1–13	46 mV per pH	300	—	ALD	130
	CNT + Ni	3	2–10	59 mV per pH	9	—	Electrodeposition	136
	Pentacene	100	2.5–7	5 V per pH	—	—	Vacuum sublimation	203 and 204
Chemo-resistor	Parylene C	1.5	4–10	23 mV per pH	<5	Drift = 18 mV h <sup>-1</sup>	CVD + O <sub>2</sub> plasma treatment	137
	Pd	2	4–10	5% per pH	100	—	DC sputtering	140
	TiO <sub>2</sub>	1	2–12	6 nS per pH	—	Stable >60 s	Electrospinning and hydrothermal deposition	139

Table 2 (Contd.)

Structure	Sensing material	Operation voltage [V]	Detection range [pH unit]	Sensitivity	Response time [s]	Stability	Fabrication of sensing materials	Ref.
	Graphene	3	4–10	2000 $\Omega$ per pH	20	—	Mechanical exfoliation of bulk graphite with scotch tape, annealing at 200 °C	138
	CNT	—	5–9	65 $\Omega$ per pH	—	—	Vacuum filtration of aqueous solution	141
	CNT + Ni	—	2–10	1% per pH	—	Stable >1 day	CNT: LPCVD at 780 °C; Ni: electrodeposition	205
ECT	P3HT	2	4–10	10 nA per pH	—	Stable for 12 h	Spin coating	144
	PEDOT:PSS	0.4	—	64 mV per pH	10	—	Spin coating; annealing at 200 °C	145
	CNT + PAA	1	2–12	73 mS per pH	—	Stable >120 days	Electropolymerisation	62
EGFET	ZnO + Pd/Au	2	7–9	—	—	—	Hydrothermal deposition	149
	CNT	0.6	3–8	27 mV per pH	40	—	Spin coating	150
	Graphene	2	2–12	100 mV per pH	—	—	High temperature growth (1100 °C)	153
	Graphene	0.4	4.3–9.4	22 mV per pH	—	—	CVD at 1000 °C, low temperature transferring, anneal at 500 °C	151
	Reduced graphene oxide	0.7	4–8	34 mV per pH	—	—	Graphene oxide prepared from Hummers method, spin coating, reducing with hydrazine at 70 °C	206
	Reduced graphene oxide	1.6	6–9	29 mV per pH	—	—	Self-assembly and reduction of graphene oxide nanosheets, annealing at 200 °C	152
	P3HT	0.6	3–8	28 mV per pH	20	—	Spin coating	150
FET	$\alpha$ 6T	0.8	2–7	—	—	Drift by 10% in 3 h	Thermal evaporation	207
	Si	0.8	4–10	68 mV per pH	—	Drift = 27 mV h <sup>-1</sup>	Deep-UV lithography, chemical-mechanical polishing, annealing at 1000 °C, wet etching	159
	DDFTTF	2	3–11	50 nA per pH	90	Stable >10 <sup>4</sup> measurement cycles	Thermal evaporation	160

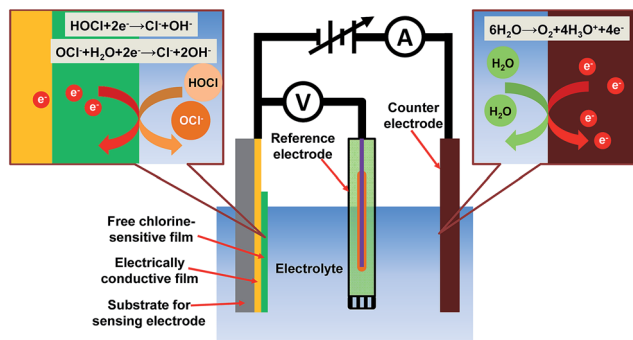


Fig. 9 Schematic of an amperometric free chlorine sensor and its sensing mechanism.

about 100 s, which was longer than the signal stabilization time of 20 s. Olivé-Monllau *et al.* developed a stable free chlorine sensor using a similar structure and fabrication process.<sup>163</sup> The resulting sensitivity of 0.23  $\mu\text{A}$  per ppm in the concentration range of 0.2 to 5 ppm makes this sensor suitable for monitoring the free chlorine level in swimming pools (lifetime >10 days, applied potential = 0.35 V). Moreover, a lower detection limit of 0.08 ppm were realized using 0.15 V applied potential on Au electrode.<sup>59</sup> The sensor maintained a stable sensitivity of 68.8 nA per ppm for over 7 days.

Pt electrodes were also used to detect free chlorine concentration and they showed similar performance to those with Au electrodes.<sup>58,164</sup> The operation voltage of a Pt electrode is higher than that of a Au electrode because the reduction of free chlorine at a Pt electrode happens at a higher potential. Another reason for the higher potential is to minimize the overlap of oxygen and hypochlorite reduction peaks, which is required for precise measurements.<sup>59</sup>

For electrodes made of materials other than noble metals, carbon has been studied due to its chemical stability. Screen printed carbon electrode coated with potassium iodide exhibited a sensing range up to 20 ppm for free chlorine, with a sensitivity of 0.2  $\mu\text{A}$  per ppm.<sup>165</sup> The sensing mechanism was based on the reaction between chlorine and iodide ions, which produced tri-iodide ions that could be titrated using sodium thiosulphate. Polymelamine has been electropolymerized onto carbon electrode to detect from 5.5  $\mu\text{M}$  to 7 mM free chlorine (sensitivity of 58  $\mu\text{A mM}^{-1}$ ).<sup>166</sup> Such an electrode exhibited an enhanced reduction peak current, which was attributed to the

reduction of the azo group ( $-\text{N}=\text{N}-$ ) and then oxidized by free chlorine in a cyclic manner. Free chlorine concentration in swimming pool water and tap water was measured using the polymelamine/carbon-based sensors.

In another study, a boron-doped diamond electrode showed reduced fouling rates compared to carbon electrodes.<sup>167</sup> The free chlorine electrodes made of this material exhibited a lifetime over 3 months. Recently, benzethonium chloride was used in electrochemical deposition of Prussian blue for a higher surface coverage on glassy carbon electrodes.<sup>168</sup> Free chlorine concentration between 9 ppb and 10 ppm could be detected in a short time (<5 s) with a sensitivity of 12  $\mu\text{A cm}^{-2}$  per ppm. This is believed to be the first publication reporting free chlorine measurement results for real water samples (tap water) using laboratory-fabricated sensors. This sensor demonstrated a measurement accuracy over 93%. Finally, ferrocene compounds were also electrochemically deposited on glassy carbon electrodes to measure the concentration of  $\text{ClO}^-$ .<sup>169</sup> However, their responses were not linear, making it difficult for use in real sensing applications. Recently, copper oxide (CuO) nanoparticles were mixed with multi-wall CNTs in an epoxy matrix as an amperometric electrode for free chlorine measurement.<sup>170</sup> CuO nanoparticles and CNTs increased the electrocatalytic active areas of the working electrode so that the electron transfer in the reduction of hypochlorite was promoted. In this study, a low detection limit of around 0.6 ppb and high sensitivity of 446 nA per ppm was realized.

#### 4.3 Challenges in developing microfabricated electrochemical free chlorine sensor

It can be noted that microfabricated electrochemical free chlorine sensors are not as well developed as pH sensors. The major challenge is the lack of reversible sensing materials for HOCl or  $\text{OCl}^-$ . A promising electrochemical sensing material should either react with free chlorine in a reversible manner, or selectively transport HOCl or  $\text{OCl}^-$  to the target substrate. The chemical reagents used in optical detection techniques (such as DPD) can react with free chlorine, but the process is irreversible. While ion-selective transport membrane exists for many ions, very few were found for HOCl or  $\text{OCl}^-$  due to their oxidizing nature. Therefore, developing advanced materials for free chlorine sensing is urgently needed.

The limitation in sensing material forces the utilization of amperometric electrodes for electrochemical sensing of free

Table 3 Comparison of conventional and microfabricated electrochemical free chlorine sensors

	Advantages	Disadvantages
Conventional electrochemical free chlorine sensors	(1) Accurate (2) Fast response	(1) Interference from pH, pressure, flow rate, and temperature (2) Large size and difficult in integration
Microfabricated electrochemical free chlorine sensors	(1) Eliminate electrolyte replenishment (2) Small (3) Low-cost (4) Easy integration with other sensors	(1) Limited lifetime of coated membrane (2) Low accuracy

Table 4 Summary of microfabricated electrochemical free chlorine sensors

Structure	Electrode/sensing material	Operation voltage [V]	Detection range [ppm]	Sensitivity	Response time [s]	Stability	Fabrication of sensing materials	Ref.
Amperometric	Au	0.15	>0.08	13.69 $\mu\text{A cm}^{-2}$ per ppm	—	Stable >7 days	Evaporation + lift-off	59
	Au	—	1.5–8	69.2 $\mu\text{A cm}^{-2}$ per ppm	20	—	Au evaporation, electrochemical deposition of Ag/AgCl	208
Chemo-resistor	Au	0.35	0.2–5	14.20 $\mu\text{A cm}^{-2}$ per ppm	120	Stable >10 days	Standard photolithography	163
	Pt	0.7	<1.5	8.00 $\mu\text{A cm}^{-2}$ per ppm <sup>a</sup>	—	Stable >5 h	RF sputtering	164
	Pt	1.2	4–400	—	—	—	—	58
	Carbon + KI	—	<20	2.08 $\mu\text{A cm}^{-2}$ per ppm	30	—	Screen printing of carbon electrodes, dispensing of KI	165
Chemo-resistor	Carbon + polymelamine Boron-doped diamond	1.2 1.4	0.4–521 ppm 0.1–100	3.98 $\mu\text{A cm}^{-2}$ per ppm 0.74 $\mu\text{A cm}^{-2}$ per ppm	—	Stable >7 days Stable >3 months	Electropolymerization Microwave plasma-assisted CVD + anodization	166 167
	Benzethonium chloride + Prussian blue on glassy carbon CuO nanoparticle mixed with MWCNT in epoxy PCAT-SWCNT	1.25 0.35 0.8	0.009–10 >0.0006 0.06–60	12.30 $\mu\text{A cm}^{-2}$ per ppm 16.07 $\mu\text{A cm}^{-2}$ per ppm 91.50 nA per dec	<5 30 <300	Stable for 15 test cycles (6 h) Stable >7 days Stable >30 h	Electrodeposition Manual casting + surface polishing Drop casting of SWCNT, flow-through adsorption of PCAT	168 170 176

<sup>a</sup> Data for electrode surface area was not given.

chlorine. Normally, cyclic voltammetry measurement has to be done first to determine the optimized voltage bias for amperometric measurement, which increases the difficulty in using the sensors. Moreover, dissolved oxygen is electroactive in the usual voltage range between +1 and –1 V for amperometric sensing of free chlorine. The interference from dissolved oxygen decreases the sensing accuracy. Finally, the requirement of a potentiostat for an amperometric sensor increases the complexity as well as the cost of the sensor. Hence, alternative sensor configurations are needed when a suitable sensing material is available. Once the above challenges are properly addressed, the concern for free chlorine sensors would become similar to those for pH sensors. Such concerns include the improvement of reliability and the reduction of fabrication costs.

#### 4.4 Summary for microfabricated electrochemical free chlorine sensor

The literature on electrochemical free chlorine sensors is limited. Within the limited scope, the amperometric sensors have been identified as the widely used structure for the electrochemical detection of free chlorine. The comparison between conventional electrochemical free chlorine sensor and microfabricated ones is given in Table 3.

A list of microfabricated electrochemical free chlorine sensors are provided in Table 4 with their structures, electrode/sensing materials, key performance parameters, and corresponding fabrication processes. The comparison shows that more works were focused on the optimization of working electrodes than the development of active sensing materials. Although microfabricated free chlorine sensors can be developed for cost-effective applications, their sensitivity varies widely and they are less accurate and reliable than the conventional sensors. This indicates that the microfabricated electrochemical free chlorine sensor is a challenging area of research that requires further intensive investigations.

## 5 Conclusions and future perspectives

Microfabricated electrochemical pH and free chlorine sensors are emerging for online monitoring of water quality due to their high sensitivity, fast response, small dimensions, ease of use, and low cost. In this paper, we reviewed microfabricated electrochemical pH and free chlorine sensors with different physical structures. We also compared these sensors from multiple aspects including sensing mechanisms, applicable materials, performance parameters, and fabrication technologies. Current challenges in developing both types of sensors were discussed. High sensitivity was reported for many microfabricated electrochemical pH sensors. However, the performance of microfabricated free chlorine sensors requires significant improvements if they are to be used for water quality monitoring.

Future work in developing novel sensing devices and systems for pH and free chlorine monitoring should consider the following: the development of advanced sensing materials, the application of innovative device structures, the implementation

of low-cost fabrication technologies, and the utilization of smart methods for sensor operation. Here, these perspectives are discussed.

### 5.1 Innovative sensor structure

Dual-gate transistors have been developed to exceed the Nernst-limit (59.16 mV per pH) in pH detection. A dual-gate transistor can be considered as an ISFET with another gate at the bottom of the semiconductor, separated by another dielectric layer. The sensitivity can be enhanced by tuning the ratio of the top and bottom gate capacitances.<sup>120,171</sup> The increased sensitivity (over 100 mV per pH) is beneficial for the detection of small pH changes.<sup>172–175</sup> In terms of free chlorine sensors, a chemoresistor was recently fabricated in contrast to conventional amperometric sensors.<sup>176</sup> The resistor consisted of single-wall CNTs modified by phenyl capped aniline tetramer (PCAT), which could be oxidized by the free-chlorine and alter the resistivity of CNTs. The highlight of this study was the high reversibility of the sensor, which was attributed to the electrochemical re-activation of the sensing material.

### 5.2 Low-cost fabrication technologies

Solution-based process is emerging for low-cost sensor applications. The need for low processing temperatures in an ambient environment is compatible with cheap polymeric substrates.<sup>177,178</sup> Typically, drop-on-demand printing technologies are attractive due to its ease in patterning and deposition of dissimilar materials. Inkjet-printed Au and Ag electrodes have been used for plating of PANI and AgCl as pH sensing electrodes and reference electrodes, respectively.<sup>179</sup> The cost of the printed Au electrode was as low as 0.04 euro per cm<sup>2</sup>. Another study proposed that Ag/AgCl reference electrodes could be fully printed in the near future.<sup>180</sup> Other low-cost fabrication technologies are also available,<sup>181</sup> which can potentially be adopted in pH and free chlorine sensors.

### 5.3 Smart operation of sensors

High performance sensing systems can be realized using improved sensing methodologies. For example, in a differential sensing system, two sets of sensors are connected to a differential amplifier. The measurement accuracy of such system under suboptimal conditions with temperatures changes or large measurement noise can be improved.<sup>182–184</sup> Another approach to improve the repeatability of potentiometric sensors is to stabilize the standard electrode potential ( $E^0$  in the Nernst equation) by short circuiting the sensing and reference electrode prior to the measurement.<sup>185</sup> Such simple adoption enables the shifting of  $E^0$  to zero, which is demanding for a calibration-free sensor.

### 5.4 Advanced sensing materials

The development of new sensing materials is of fundamental importance in sensors, especially for health and environmental monitoring, and it has recently been reviewed by several groups.<sup>8,35,36,186</sup> Therefore, only a brief discussion is given here.

- Nanomaterials, such as CNTs, graphene, and nanostructured metal oxides, are emerging in the development of pH and free chlorine sensors. The large surface-to-volume ratio of nanomaterials can enhance the charge transfer ability of the sensing material, hence improve the sensitivity of a potentiometric sensor. The large surface area of nanomaterials may provide enough room for numerous surface binding sites for sensing using an ISFET. The high catalytic activity of metal (*e.g.* Ag, Pd, and Pt) nanoparticles may enable new means to detect free chlorine in water.

- Biocompatible and eco-friendly sensing materials are preferred in future. Since the sensors are in contact with the water distribution system, any hazardous substances (*e.g.* heavy metals, neurotoxins, *etc.*) must be carefully applied to protect the nature and human being. Also, the biocompatible sensing materials may be used to measure the pH of bodily fluid, therefore, will find wide applications in health monitoring. The materials should be highly sensitive and reliable in the range from strong acid (pH = 1–3.5 for gastric secretion) to mild alkaline (pH ~ 8 for pancreatic secretion).

- The stability of sensing materials requires to be improved for reliable sensor operation in the aqueous environment (in contrast to disposable sensors). Such materials should be chemically inert (except for the reactions with the target analyte), mechanically robust, anti-fouling, and have little water absorption in order to keep the output electrical signal stable for months. This perspective is especially important for free chlorine sensors because their analyte is highly oxidizing.

- Currently, some of the pH sensitive materials, such as partially hydrated  $\text{IrO}_x$ ,  $\text{RuO}_2$  and  $\text{PdO}$  show super-Nernst response. However, in order to realize pH sensors with improved reproducibility and reliability using these oxides, good control of the ratio of hydrated and non-hydrated oxides during their synthesis is needed.

- The processability and cost of the new sensing materials would be critical. The materials could either be chosen from existing commercial products (*e.g.* use drawing pencils to replace glassy carbon electrodes), or should be compatible with low-cost processing technologies such as printing.

The foundation of the emerging microfabricated electrochemical pH and free chlorine sensing systems would be the development of new materials with high sensitivity, selectivity, and stability. With the use of newly developed materials, the physical configurations of sensors need to be properly designed to transduce the chemical signal to readable electronic outputs. Finally, cost effective microfabrication technologies as well as systems designs are needed to bridge theoretical concepts with real world applications.

## Acknowledgements

This research is supported by Discovery Grants from the Natural Science and Engineering Research Council of Canada, an infrastructure grant from the Canada Foundation for Innovation, an Ontario Research Fund for Research Excellence Funding Grant, a FedDev of Southern Ontario grant, the Canada

Research Chair program, NSERC ResEau strategic network and the NCE IC-IMPACTS.

## Notes and references

- USEPA, *WaterSentinel online water quality monitoring as an indicator of drinking water contamination*, EPA 817-D-05-002, Washington, D.C., U.S. Environmental Protection Agency, Water Security Division, 2005, [http://www.epa.gov/watersecurity/pubs/watersentinel\\_wq\\_monitoring.pdf](http://www.epa.gov/watersecurity/pubs/watersentinel_wq_monitoring.pdf), accessed 21 October 2014.
- W. F. Boron, *Medical physiology: A cellular and molecular approach*, Saunders/Elsevier, Philadelphia, PA, USA, 2003.
- WHO, *Guidelines for drinking-water quality - Second edition - Volume 2-Health criteria and other supporting information*, Geneva, 1996, [http://www.who.int/water\\_sanitation\\_health/dwq/2edvol2p1.pdf](http://www.who.int/water_sanitation_health/dwq/2edvol2p1.pdf), accessed 21 October 2014.
- Health Canada, *Guidelines for Canadian drinking water quality: Chlorine*, Authority of the Minister of Health, Ottawa, Canada, 2009, <http://www.hc-sc.gc.ca/ewh-semt/pubs/water-eau/chlorine-chlore/index-eng.php>, accessed 21 October 2014.
- USEPA, *Nitrification*, Office of Water, Washington, D.C., USA, 2002, <http://water.epa.gov/lawsregs/rulesregs/sdwa/tcr/upload/nitrification.pdf>, accessed 1 March 2015.
- L. M. Prescott, J. P. Harley and D. A. Klein, *The influence of environmental factors on growth*, *Microbiology*, McGraw-Hill Companies Inc., USA, 1999.
- Health impact of acidic deposition, Science of the total environment*, World Health Organization Working Group, 1986.
- O. Korostynska, K. Arshak, E. Gill and A. Arshak, *IEEE Sens. J.*, 2008, **8**, 20–28.
- R. Sadiq, S. Imran and V. Kleiner, *Examining the impact of water quality on the integrity of distribution infrastructure*, American Water Works Association Research Foundation, Denver, CO, USA, 2007.
- P. Payment, M. Waite and A. Durfour, *Assessing microbial safety of drinking water improving approaches and methods: improving approaches and methods*, Organisation for Economic Cooperation and Development and World Health Organization, 2003.
- M. H. Banna, S. Imran, A. Francisque, H. Najjaran, R. Sadiq, M. Rodriguez and M. Hoorfar, *Crit. Rev. Environ. Sci. Technol.*, 2014, **44**, 1370–1421.
- G. Connell, *Water disinfection series: the chlorination/chloramination handbook*, American Water Works Association, Denver, CO, USA, 1996.
- WHO, *Guidelines for drinking-water quality, Third edition*, Geneva, 2008, [http://www.who.int/water\\_sanitation\\_health/dwq/fulltext.pdf](http://www.who.int/water_sanitation_health/dwq/fulltext.pdf), accessed 21 October 2014.
- USEPA, *National primary drinking water regulations*, Washington, D.C., USA, 2009, <http://www.epa.gov/ogwdw/consumer/pdf/mcl.pdf>, accessed 21 October 2014.
- USEPA, *Edition of the drinking water standards and health advisories*, Office of Water, Washington, D.C., USA, 2012, <http://water.epa.gov/action/advisories/drinking/upload/dwstandards2012.pdf>, accessed 21 October 2014.
- P. Guyer, *An Engineering SoundBite: Water Treatment*, Guyer Partners, 2010.
- Chlorine measurement by amperometric sensor, Application Data Sheet, ADS 43-6063/rev.B*, Emerson Process Management, 2009, [http://www2.emersonprocess.com/siteadmincenter/PM%20Rosemount%20Analytical%20Documents/Liq\\_ADS\\_43-6063.pdf](http://www2.emersonprocess.com/siteadmincenter/PM%20Rosemount%20Analytical%20Documents/Liq_ADS_43-6063.pdf), accessed 21 October 2014.
- M. Badihi-Mossberg, V. Buchner and J. Rishpon, *Electroanalysis*, 2007, **19**, 2015–2028.
- N. Jaffrezic-Renault and S. V. Dzyadevych, *Sensors*, 2008, **8**, 2569–2588.
- G. Hanrahan, D. G. Patil and J. Wang, *J. Environ. Monit.*, 2004, **6**, 657–664.
- Y. Miao, J. Chen and K. Fang, *J. Biochem. Biophys. Methods*, 2005, **63**, 1–9.
- V. B. Malkov, B. Zachman and T. Scribner, *presented in part at the Water Quality Technology Conference and Exposition*, Seattle, WA, USA, 15–19 November 2009.
- M. M. R. Howlader, P. R. Selvaganapathy, M. J. Deen and T. Suga, *IEEE J. Sel. Top. Quantum Electron.*, 2011, **17**, 689–703.
- M. M. Howlader, M. J. Deen and T. Suga, *Jpn. J. Appl. Phys.*, 2015, **54**, 030201.
- Y. Zhang, H.-F. Ji, D. Snow, R. Sterling and G. M. Brown, *Instrum. Sci. Technol.*, 2004, **32**, 361–369.
- Q. Thong Trinh, G. Gerlach, J. Sorber and K.-F. Arndt, *Sens. Actuators, B*, 2006, **117**, 17–26.
- G. Gerlach, M. Guenther, J. Sorber, G. Suchaneck, K.-F. Arndt and A. Richter, *Sens. Actuators, B*, 2005, **111**, 555–561.
- M. H. Banna, H. Najjaran, R. Sadiq, S. A. Imran, M. J. Rodriguez and M. Hoorfar, *Sens. Actuators, B*, 2014, **193**, 434–441.
- M. J. Deen and P. K. Basu, *Silicon Photonics: Fundamentals and Devices*, John Wiley & Sons, Chichester, UK, 2012.
- M. J. Deen, B. Iñiguez, O. Marinov and F. Lime, *J. Mater. Sci.: Mater. Electron.*, 2006, **17**, 663–683.
- M. J. Deen and F. Pascal, *J. Mater. Sci.: Mater. Electron.*, 2006, **17**, 549–575.
- Z. Cheng, M. J. Deen and H. Peng, *IEEE Transactions on Biomedical Circuits and Systems*, 2015, 1–10.
- D. Wencel, T. Abel and C. McDonagh, *Anal. Chem.*, 2014, **86**, 15–29.
- W. Vonau and U. Guth, *J. Solid State Electrochem.*, 2006, **10**, 746–752.
- P. Kurzweil, *Sensors*, 2009, **9**, 4955–4985.
- O. Korostynska, K. Arshak, E. Gill and A. Arshak, *Sensors*, 2007, **7**, 3027–3042.
- M. W. Shinwari, D. Zhitomirsky, I. A. Deen, P. R. Selvaganapathy, M. J. Deen and D. Landheer, *Sensors*, 2010, **10**, 1679–1715.
- C. Liao and F. Yan, *Polym. Rev.*, 2013, **53**, 352–406.
- M. Ates, *Mater. Sci. Eng., C*, 2013, **33**, 1853–1859.
- J. T. Mabeck and G. G. Malliaras, *Anal. Bioanal. Chem.*, 2006, **384**, 343–353.

- 41 T. Someya, A. Dodabalapur, J. Huang, K. C. See and H. E. Katz, *Adv. Mater.*, 2010, **22**, 3799–3811.
- 42 U. Lange, N. V. Roznyatovskaya and V. M. Mirsky, *Anal. Chim. Acta*, 2008, **614**, 1–26.
- 43 D. Elkington, N. Cooling, W. Belcher, P. C. Dastoor and X. Zhou, *Electronics*, 2014, **3**, 234–254.
- 44 C. Bartic and G. Borghs, *Anal. Bioanal. Chem.*, 2006, **384**, 354–365.
- 45 D. S. Tarbell and A. T. Tarbell, *J. Chem. Educ.*, 1980, **57**, 133.
- 46 F. Haber and Z. Klemensiewicz, *Z. Phys. Chem.*, 1909, **67**, 385–431.
- 47 R. P. Buck, S. Rondinini, A. K. Covington, F. G. K. Baucke, C. Brett, M. F. Camoes, M. J. T. Milton, T. Mussini, R. Naumann and K. W. Pratt, *Pure Appl. Chem.*, 2002, **74**, 2169–2200.
- 48 J. C. Morris, *Health perspective in the oxidative treatment of water for potable supply. Part 2. Health assessment of current oxidant-disinfectants*, National Institute for Water Supply, Leidschendam, The Netherlands, 1982.
- 49 J. C. Morris, *J. Phys. Chem.*, 1966, **70**, 3798–3805.
- 50 G. Gordon, D. L. Sweetin, K. Smith and G. E. Pacey, *Talanta*, 1991, **38**, 145–149.
- 51 J. D. Johnson and R. Overby, *Anal. Chem.*, 1969, **41**, 1744–1750.
- 52 M. Zenki, H. Komatsubara and K. Tōei, *Anal. Chim. Acta*, 1988, **208**, 317–320.
- 53 K. K. Verma, A. Jain and A. Townshend, *Anal. Chim. Acta*, 1992, **261**, 233–240.
- 54 S. G. Dmitrienko, O. A. Sviridova, L. N. Pyatkova, V. A. Zhukova and Y. A. Zolotov, *Anal. Chim. Acta*, 2000, **405**, 231–237.
- 55 G. C. White, *Handbook of chlorination*, Van Nostrand Reinhold Company, New York, NY, USA, 1986.
- 56 J. Ellis and P. L. Brown, *Anal. Chim. Acta*, 1981, **124**, 431–436.
- 57 T. Nakagama, M. Yamada and T. Hobo, *Anal. Chim. Acta*, 1990, **231**, 7–12.
- 58 F. Kodera, M. Umeda and A. Yamada, *Anal. Chim. Acta*, 2005, **537**, 293–298.
- 59 F. J. D. Campo, O. Ordeig and F. J. Muñoz, *Anal. Chim. Acta*, 2005, **554**, 98–104.
- 60 A. Fog and R. P. Buck, *Sens. Actuators*, 1984, **5**, 137–146.
- 61 P. Bergveld, *Sens. Actuators, B*, 2003, **88**, 1–20.
- 62 P. Gou, N. D. Kraut, I. M. Feigel, H. Bai, G. J. Morgan, Y. Chen, Y. Tang, K. Bocan, J. Stachel and L. Berger, *Sci. Rep.*, 2014, **4**, 4468.
- 63 P. Gupta, S. K. Yadav, B. Agrawal and R. N. Goyal, *Sens. Actuators, B*, 2014, **204**, 791–798.
- 64 D. K. Kampouris, R. O. Kadara, N. Jenkinson and C. E. Banks, *Anal. Methods*, 2009, **1**, 25–28.
- 65 N. Mzoughi, A. Abdellah, Q. Gong, H. Grothe, P. Lugli, B. Wolf and G. Scarpa, *Sens. Actuators, B*, 2012, **171**, 537–543.
- 66 L.-M. Kuo, K.-N. Chen, Y.-L. Chuang and S. Chao, *ECS Solid State Lett.*, 2013, **2**, P28–P30.
- 67 M. A. Rahman, P. Kumar, D.-S. Park and Y.-B. Shim, *Sensors*, 2008, **8**, 118–141.
- 68 S. Safari, P. R. Selvaganapathy and M. J. Deen, *J. Electrochem. Soc.*, 2013, **160**, B177–B183.
- 69 S. Safari, P. R. Selvaganapathy, A. Derardja and M. J. Deen, *Nanotechnology*, 2011, **22**, 315601.
- 70 W.-D. Huang, H. Cao, S. Deb, M. Chiao and J.-C. Chiao, *Sens. Actuators, A*, 2011, **169**, 1–11.
- 71 S. Yao, M. Wang and M. Madou, *J. Electrochem. Soc.*, 2001, **148**, H29–H36.
- 72 H.-J. Chung, M. S. Sulkin, J.-S. Kim, C. Goudeseune, H.-Y. Chao, J. W. Song, S. Y. Yang, Y.-Y. Hsu, R. Ghaffari and I. R. Efimov, *Adv. Healthcare Mater.*, 2014, **3**, 59–68.
- 73 T. Y. Kim and S. Yang, *Sens. Actuators, B*, 2014, **196**, 31–38.
- 74 C. M. Nguyen, S. Rao, Y.-S. Seo, K. Schadt, Y. Hao and J.-C. Chiao, *IEEE Trans. Nanotechnol.*, 2014, **13**, 945–953.
- 75 L.-M. Kuo, Y.-C. Chou, K.-N. Chen, C.-C. Lu and S. Chao, *Sens. Actuators, B*, 2014, **193**, 687–691.
- 76 J. Park, M. Kim and S. Kim, *Sens. Actuators, B*, 2014, **204**, 197–202.
- 77 S. Zaman, M. H. Asif, A. Zainelabdin, G. Amin, O. Nur and M. Willander, *J. Electroanal. Chem.*, 2011, **662**, 421–425.
- 78 M. Hussain, Z. H. Ibupoto, M. A. Abbasi, O. Nur and M. Willander, *J. Electroanal. Chem.*, 2014, **717**, 78–82.
- 79 L. Santos, J. P. Neto, A. Crespo, D. Nunes, N. Costa, I. M. Fonseca, P. Barquinha, L. Pereira, J. Silva and R. Martins, *ACS Appl. Mater. Interfaces*, 2014, **6**, 12226–12234.
- 80 A. Sardarinejad, D. K. Maurya and K. Alameh, *Sens. Actuators, A*, 2014, **214**, 15–19.
- 81 H. Arida, *Microchim. Acta*, 2014, 1–8.
- 82 Y. Qin, A. U. Alam, S. Pan, M. M. R. Howlader, R. Ghosh, P. R. Selvaganapathy, Y. Wu and M. J. Deen, *Talanta*, 2015, submitted.
- 83 T. Lindfors and A. Ivaska, *J. Electroanal. Chem.*, 2002, **531**, 43–52.
- 84 B. Lakard, G. Herlem, S. Lakard, R. Guyetant and B. Fahys, *Polymer*, 2005, **46**, 12233–12239.
- 85 B. Lakard, O. Segut, S. Lakard, G. Herlem and T. Gharbi, *Sens. Actuators, B*, 2007, **122**, 101–108.
- 86 A. J. Bandodkar, V. W. S. Hung, W. Jia, G. Valdés-Ramírez, J. R. Windmiller, A. G. Martínez, J. Ramírez, G. Chan, K. Kerman and J. Wang, *Analyst*, 2013, **138**, 123–128.
- 87 T. Guinovart, G. Valdés-Ramírez, J. R. Windmiller, F. J. Andrade and J. Wang, *Electroanalysis*, 2014, **26**, 1345–1353.
- 88 W. Prissanaroon-Ouajai, P. J. Pigram, R. Jones and A. Sirivat, *Sens. Actuators, B*, 2008, **135**, 366–374.
- 89 T. Trantidou, D. J. Payne, V. Tsiligkiridis, Y.-C. Chang, C. Toumazou and T. Prodromakis, *Sens. Actuators, B*, 2013, **186**, 1–8.
- 90 M. M. R. Howlader, T. Suga, A. Takahashi, K. Saijo, S. Ozawa and K. Nanbu, *J. Mater. Sci.*, 2005, **40**, 3177–3184.
- 91 M. M. R. Howlader, M. Iwashita, K. Nanbu, K. Saijo and T. Suga, *IEEE Trans. Adv. Packag.*, 2005, **28**, 495–502.
- 92 M. M. R. Howlader, T. E. Doyle, S. Mohtashami and J. R. Kish, *Sens. Actuators, B*, 2013, **178**, 132–139.
- 93 M. M. R. Howlader, A. U. Alam, R. P. Sharma and M. J. Deen, *Phys. Chem. Chem. Phys.*, 2015, **17**, 10135–10145.

- 94 C. A. Li, K. N. Han, X.-H. Pham and G. H. Seong, *Analyst*, 2014, **139**, 2011–2015.
- 95 M. W. Shinwari and M. J. Deen, *J. Electrochem. Soc.*, 2011, **158**, J189–J194.
- 96 M. W. Shinwari, M. J. Deen and P. Selvaganapathy, *IET Circuits, Devices and Systems*, 2008, **2**, 158–165.
- 97 M. W. Shinwari, M. J. Deen and D. Landheer, *Microelectron. Reliab.*, 2007, **47**, 2025–2057.
- 98 M. J. Deen, M. W. Shinwari, J. C. Ranuárez and D. Landheer, *J. Appl. Phys.*, 2006, **100**, 074703.
- 99 D. Landheer, W. R. McKinnon, G. Aers, W. Jiang, M. J. Deen and M. W. Shinwari, *IEEE Sens. J.*, 2007, **7**, 1233–1242.
- 100 P. D. Batista and M. Mulato, *Appl. Phys. Lett.*, 2005, **87**, 143508.
- 101 J. C. Chou and L. P. Liao, *Jpn. J. Appl. Phys.*, 2004, **43**, 61–65.
- 102 J.-C. Chou and L. P. Liao, *Thin Solid Films*, 2005, **476**, 157–161.
- 103 P.-K. Shin, *Appl. Surf. Sci.*, 2003, **214**, 214–221.
- 104 T. Mikolajick, R. Kühnhold and H. Ryssel, *Sens. Actuators, B*, 1997, **44**, 262–267.
- 105 M. Chen, Y. Jin, X. Qu, Q. Jin and J. Zhao, *Sens. Actuators, B*, 2014, **192**, 399–405.
- 106 C. H. Kao, H. Chen, M. L. Lee, C. C. Liu, H.-Y. Ueng, Y. C. Chu, Y. J. Chen and K. M. Chang, *J. Appl. Phys.*, 2014, **115**, 184701.
- 107 K. Bedner, V. A. Guzenko, A. Tarasov, M. Wipf, R. L. Stoop, D. Just, S. Rigante, W. Fu, R. A. Minamisawa and C. David, *Sens. Mater.*, 2013, **25**, 567–576.
- 108 C.-M. Yang, C.-Y. Wang and C.-S. Lai, *J. Vac. Sci. Technol., B*, 2014, **32**, 03D113.
- 109 T.-M. Pan, P.-Y. Liao, K.-Y. Chang and L. Chi, *Electrochim. Acta*, 2013, **89**, 798–806.
- 110 K. Niigata, K. Narano, Y. Maeda and J.-P. Ao, *Jpn. J. Appl. Phys.*, 2014, **53**, 11RD01.
- 111 K. Kim, T. Rim, C. Park, D. Kim, M. Meyyappan and J.-S. Lee, *Nanotechnology*, 2014, **25**, 345501.
- 112 S. Upadhyay, R. Frederiksen, N. Lloret, L. De Vico, P. Krogstrup, J. H. Jensen, K. L. Martinez and J. Nygård, *Appl. Phys. Lett.*, 2014, **104**, 203504.
- 113 T.-E. Bae, H. Kim, J. Jung and W.-J. Cho, *Appl. Phys. Lett.*, 2014, **104**, 153506.
- 114 I. Fakih, S. Sabri, F. Mahvash, M. Nannini, M. Siaj and T. Szkopek, *Appl. Phys. Lett.*, 2014, **105**, 083101.
- 115 S. Ritjareonwattu, Y. Yun, C. Pearson and M. C. Petty, *IEEE Sens. J.*, 2012, **12**, 1181–1186.
- 116 S. Ritjareonwattu, Y. Yun, C. Pearson and M. C. Petty, *Org. Electron.*, 2010, **11**, 1792–1795.
- 117 J. Kofler, K. Schmoltnner, A. Klug and E. J. W. List-Kratochvil, *Appl. Phys. Lett.*, 2014, **104**, 193305.
- 118 A. Loi, I. Manunza and A. Bonfiglio, *Appl. Phys. Lett.*, 2005, **86**, 103512.
- 119 M. Yun, A. Sharma, C. Fuentes-Hernandez, D. K. Hwang, A. Dindar, S. Singh, S. Choi and B. Kippelen, *ACS Appl. Mater. Interfaces*, 2014, **6**, 1616–1622.
- 120 M.-J. Spijkman, J. J. Brondijk, T. C. T. Geuns, E. C. P. Smits, T. Cramer, F. Zerbetto, P. Stoliar, F. Biscarini, P. W. M. Blom and D. M. de Leeuw, *Adv. Funct. Mater.*, 2010, **20**, 898–905.
- 121 J. van der Spiegel, I. Lauks, P. Chan and D. Babić, *Sens. Actuators*, 1983, **4**, 291–298.
- 122 L. Maiolo, S. Mirabella, F. Maita, A. Alberti, A. Minotti, V. Strano, A. Pecora, Y. Shacham-Diamand and G. Fortunato, *Appl. Phys. Lett.*, 2014, **105**, 093501.
- 123 J.-C. Chou and C.-W. Chen, *IEEE Sens. J.*, 2009, **9**, 277–284.
- 124 J.-L. Chiang, J.-C. Chou and Y.-C. Chen, *J. Med. Biol. Eng.*, 2001, **21**, 135–146.
- 125 P.-C. Yao, J.-L. Chiang and M.-C. Lee, *Solid State Sci.*, 2014, **28**, 47–54.
- 126 N. Vieira, A. Figueiredo, A. D. Faceto, A. A. A. de Queiroz, V. Zucolotto and F. E. G. Guimarães, *Sens. Actuators, B*, 2012, **169**, 397–400.
- 127 Y.-H. Liao and J.-C. Chou, *Mater. Chem. Phys.*, 2009, **114**, 542–548.
- 128 Y.-C. Huang, F.-S. Tsai and S.-J. Wang, *Jpn. J. Appl. Phys.*, 2014, **53**, 06JG02.
- 129 E. M. Guerra and M. Mulato, *Mater. Sci. Appl.*, 2014, **5**, 459–466.
- 130 H.-H. Li, C.-E. Yang, C.-C. Kei, C.-Y. Su, W.-S. Dai, J.-K. Tseng, P.-Y. Yang, J.-C. Chou and H.-C. Cheng, *Thin Solid Films*, 2013, **529**, 173–176.
- 131 C.-H. Kao, H. Chen, L.-T. Kuo, J.-C. Wang, Y.-T. Chen, Y.-C. Chu, C.-Y. Chen, C.-S. Lai, S. W. Chang and C. W. Chang, *Sens. Actuators, B*, 2014, **194**, 419–426.
- 132 A. Das, D. H. Ko, C.-H. Chen, L.-B. Chang, C.-S. Lai, F.-C. Chu, L. Chow and R.-M. Lin, *Sens. Actuators, B*, 2014, **205**, 199–205.
- 133 P. D. Batista and M. Mulato, *J. Mater. Sci.*, 2010, **45**, 5478–5481.
- 134 S.-C. Hung, N.-J. Cheng, C.-F. Yang and Y.-P. Lo, *Nanoscale Res. Lett.*, 2014, **9**, 502.
- 135 B.-R. Huang, S.-C. Hung and Y.-P. Lo, *Mater. Sci. Semicond. Process.*, 2014, **26**, 710–715.
- 136 B.-R. Huang and T.-C. Lin, *Appl. Phys. Lett.*, 2011, **99**, 023108.
- 137 T. Trantidou, M. Tariq, C. M. Terracciano, C. Toumazou and T. Prodromakis, *Sensors*, 2014, **14**, 11629–11639.
- 138 N. Lei, P. Li, W. Xue and J. Xu, *Meas. Sci. Technol.*, 2011, **22**, 107002.
- 139 W. S. Lee, Y.-S. Park and Y.-K. Cho, *ACS Appl. Mater. Interfaces*, 2014, **6**, 12189–12195.
- 140 Y. T. Lee, E. Lee, J. M. Lee and W. Lee, *Curr. Appl. Phys.*, 2009, **9**, e218–e221.
- 141 K. F. Lei, K.-F. Lee and S.-I. Yang, *Microelectron. Eng.*, 2012, **100**, 1–5.
- 142 P. Lin and F. Yan, *Adv. Mater.*, 2012, **24**, 34–51.
- 143 G. Tarabella, F. M. Mohammadi, N. Coppedè, F. Barbero, S. Iannotta, C. Santato and F. Cicoira, *Chem. Sci.*, 2013, **4**, 1395–1409.
- 144 G. Scarpa, A.-L. Idzko, A. Yadav and S. Thalhammer, *Sensors*, 2010, **10**, 2262–2273.
- 145 P. Lin, F. Yan and H. L. W. Chan, *ACS Appl. Mater. Interfaces*, 2010, **2**, 1637–1641.

- 146 M. J. Panzer and C. D. Frisbie, *Adv. Mater.*, 2008, **20**, 3177–3180.
- 147 A. J. Bard and L. R. Faulkner, *Electrochemical methods: fundamentals and applications*, John Wiley & Sons, New York, USA, 2nd edn, 2001.
- 148 L. Kergoat, B. Piro, M. Berggren, G. Horowitz and M.-C. Pham, *Anal. Bioanal. Chem.*, 2012, **402**, 1813–1826.
- 149 V. Pachauri, K. Kern and K. Balasubramanian, *Appl. Phys. Lett.*, 2013, **102**, 023501.
- 150 A. M. Müenzer, K. Melzer, M. Heimgreiter and G. Scarpa, *Biochim. Biophys. Acta*, 2013, **1830**, 4353–4358.
- 151 B. Maillly-Giacchetti, A. Hsu, H. Wang, V. Vinciguerra, F. Pappalardo, L. Occhipinti, E. Guidetti, S. Coffa, J. Kong and T. Palacios, *J. Appl. Phys.*, 2013, **114**, 084505.
- 152 I.-Y. Sohn, D.-J. Kim, J.-H. Jung, O. J. Yoon, T. Nguyen Thanh, T. Tran Quang and N.-E. Lee, *Biosens. Bioelectron.*, 2013, **45**, 70–76.
- 153 P. K. Ang, W. Chen, A. T. S. Wee and K. P. Loh, *J. Am. Chem. Soc.*, 2008, **130**, 14392–14393.
- 154 F. Liao, C. Chen and V. Subramanian, *Sens. Actuators, B*, 2005, **107**, 849–855.
- 155 L. Torsi and A. Dodabalapur, *Anal. Chem.*, 2005, **77**, 380A–387A.
- 156 S. Zilker, C. Detcheverry, E. Cantatore and D. M. De Leeuw, *Appl. Phys. Lett.*, 2001, **79**, 1124–1126.
- 157 O. Knopfmacher, M. L. Hammock, A. L. Appleton, G. Schwartz, J. Mei, T. Lei, J. Pei and Z. Bao, *Nat. Commun.*, 2014, **5**, 2954.
- 158 C. Feng, O. Marinov, M. J. Deen, P. R. Selvaganapathy and Y. Wu, *J. Appl. Phys.*, 2015, **117**, 185501.
- 159 J.-H. Ahn, J.-Y. Kim, M.-L. Seol, D. J. Baek, Z. Guo, C.-H. Kim, S.-J. Choi and Y.-K. Choi, *Appl. Phys. Lett.*, 2013, **102**, 083701.
- 160 M. E. Roberts, S. C. B. Mannsfeld, N. Queraltó, C. Reese, J. Locklin, W. Knoll and Z. Bao, *Proc. Natl. Acad. Sci. U. S. A.*, 2008, **105**, 12134–12139.
- 161 J. Jin, Y. Suzuki, N. Ishikawa and T. Takeuchi, *Anal. Sci.*, 2004, **20**, 205–207.
- 162 A. Mehta, H. Shekhar, S. Hyun, S. Hong and H. Cho, *Water Sci. Technol.*, 2006, **53**, 403–410.
- 163 R. Olivé-Monllau, J. Orozco, C. Fernández-Sánchez, M. Baeza, J. Bartrolí, C. Jimenez-Jorquera and F. Céspedes, *Talanta*, 2009, **77**, 1739–1744.
- 164 A. Okumura, A. Hirabayashi, Y. Sasaki and R. Miyake, *Anal. Sci.*, 2001, **17**, 1113–1115.
- 165 F. Davis, S. D. Collyer, D. D. Gornall, K. A. Law, D. W. Mills and S. P. J. Higson, *Chem. Today*, 2007, **25**, 28–31.
- 166 K. Senthilkumar and J.-M. Zen, *Electrochem. Commun.*, 2014, **46**, 87–90.
- 167 M. Murata, T. A. Ivandini, M. Shibata, S. Nomura, A. Fujishima and Y. Einaga, *J. Electroanal. Chem.*, 2008, **612**, 29–36.
- 168 P. Salazar, M. Martín, F. J. García-García, J. L. González-Mora and A. R. González-Elipe, *Sens. Actuators, B*, 2015, **213**, 116–123.
- 169 B. Wang and J.-I. Anzai, *Int. J. Electrochem. Sci.*, 2015, **10**, 3260–3268.
- 170 J. Muñoz, F. Céspedes and M. Baeza, *Microchem. J.*, 2015, **122**, 189–196.
- 171 H.-J. Jang and W.-J. Cho, *Sci. Rep.*, 2014, **4**, 5284.
- 172 I.-K. Lee, W.-J. Cho, K. H. Lee and S. Lee, *ACS Appl. Mater. Interfaces*, 2014, **6**, 22680–22686.
- 173 J.-K. Park, H.-J. Jang, J.-T. Park and W.-J. Cho, *Solid-State Electron.*, 2014, **97**, 2–7.
- 174 K. Takechi, S. Iwamatsu, T. Yahagi, Y. Abe, S. Kobayashi and H. Tanabe, *Jpn. J. Appl. Phys.*, 2014, **53**, 076702.
- 175 N. Liu, Y. H. Liu, P. Feng, L. Q. Zhu, Y. Shi and Q. Wan, *Appl. Phys. Lett.*, 2015, **106**, 073507.
- 176 L. H. H. Hsu, E. Hoque, P. Kruse and P. R. Selvaganapathy, *Appl. Phys. Lett.*, 2015, **106**, 063102.
- 177 Y. Qin, M. M. R. Howlader, M. J. Deen, Y. M. Haddara and P. R. Selvaganapathy, *Sens. Actuators, B*, 2014, **202**, 758–778.
- 178 Y. Qin, D. H. Turkenburg, I. Barbu, W. T. T. Smaal, K. Myny, W.-Y. Lin, G. H. Gelinck, P. Heremans, J. Liu and E. R. Meinders, *Adv. Funct. Mater.*, 2012, **22**, 1209–1214.
- 179 A. Määttänen, U. Vanamo, P. Ihalainen, P. Pulkkinen, H. Tenhu, J. Bobacka and J. Peltonen, *Sens. Actuators, B*, 2013, **177**, 153–162.
- 180 E. T. S. G. da Silva, S. Miserere, L. T. Kubota and A. Merkoçi, *Anal. Chem.*, 2014, **86**, 10531–10534.
- 181 A. Santos, M. J. Deen and L. F. Marsal, *Nanotechnology*, 2015, **26**, 042001.
- 182 J.-C. Chou, C.-Y. Lin, Y.-H. Liao, J.-T. Chen, Y.-L. Tsai, J.-L. Chen and H.-T. Chou, *IEEE Sens. J.*, 2014, **14**, 1405–1411.
- 183 T.-Y. Cheng, J.-C. Chou, Y.-H. Liao, Y.-L. Tsai, J.-W. Lin, C.-Y. Jhang, C.-Y. Liu, J.-E. Hu and H.-T. Chou, *presented in part at the Proceedings of the World Congress on Engineering*, London, U.K., July 3–5, 2013.
- 184 T. Miura and A. Yamada, *presented in part at the 2014 International Symposium on Micro-NanoMechatronics and Human Science (MHS)*, Nagoya, Japan, November 10–12, 2014.
- 185 U. Vanamo and J. Bobacka, *Anal. Chem.*, 2014, **86**, 10540–10545.
- 186 S. Glab, A. Hulanicki, G. Edwall and F. Ingman, *Crit. Rev. Anal. Chem.*, 1989, **21**, 29–47.
- 187 J. Chu, Y. Zhao, S.-H. Li, H.-Q. Yu, G. Liu and Y.-C. Tian, *Electrochim. Acta*, 2015, **152**, 6–12.
- 188 A. Lale, A. Tsopela, A. Civelas, L. Salvagnac, J. Launay and P. Temple-Boyer, *Sens. Actuators, B*, 2015, **206**, 152–158.
- 189 R. Zhao, M. Xu, J. Wang and G. Chen, *Electrochim. Acta*, 2010, **55**, 5647–5651.
- 190 S. M. Al-Hilli, M. Willander, A. Ost and P. Stralfors, *J. Appl. Phys.*, 2007, **102**, 084304.
- 191 D. Sharp, *Biosens. Bioelectron.*, 2013, **50**, 399–405.
- 192 E. L. Silva, A. C. Bastos, M. A. Neto, R. F. Silva, M. G. S. Ferreira, M. L. Zheludkevich and F. J. Oliveira, *Electrochem. Commun.*, 2014, **40**, 31–34.
- 193 M. Kaempgen and S. Roth, *J. Electroanal. Chem.*, 2006, **586**, 72–76.
- 194 P. C. Pandey and G. Singh, *Talanta*, 2001, **55**, 773–782.
- 195 Q. Li, H. Li, J. Zhang and Z. Xu, *Sens. Actuators, B*, 2011, **155**, 730–736.

- 196 H. Xu, Y. Pan, Y. Wang, G. Li, Y. Chen and Y. Ye, *Meas. Sci. Technol.*, 2012, **23**, 125101.
- 197 C.-M. Yang, T.-W. Chiang, Y.-T. Yeh, A. Das, Y.-T. Lin and T.-C. Chen, *Sens. Actuators, B*, 2015, **207**, 858–864.
- 198 C.-C. Chen, H.-I. Chen, H.-Y. Liu, P.-C. Chou, J.-K. Liou and W.-C. Liu, *Sens. Actuators, B*, 2015, **209**, 658–663.
- 199 S. Rigante, P. Scarbolo, M. Wipf, R. L. Stoop, K. Bedner, E. Buitrago, A. Bazigos, D. Bouvet, M. Calame and C. Schonenberger, *ACS Nano*, 2015, **9**, 4872–4881.
- 200 T.-M. Pan, C.-H. Cheng and C.-D. Lee, *J. Electrochem. Soc.*, 2009, **156**, J108–J111.
- 201 T. Ji, P. Rai, S. Jung and V. K. Varadan, *Appl. Phys. Lett.*, 2008, **92**, 233304.
- 202 J.-L. Chiang, J.-F. Hsu, S.-F. Lee, L.-Y. Lee and H.-Y. Liu, *J. Vac. Sci. Technol., B*, 2009, **27**, 1462–1465.
- 203 A. Caboni, E. Orgiu, M. Barbaro and A. Bonfiglio, *IEEE Sens. J.*, 2009, **9**, 1963–1970.
- 204 A. Caboni, E. Orgiu, E. Scavetta, M. Barbaro and A. Bonfiglio, *Appl. Phys. Lett.*, 2009, **95**, 123304.
- 205 D. Jung, M.-E. Han and G. S. Lee, *Mater. Lett.*, 2014, **116**, 57–60.
- 206 C. Reiner-Rozman, M. Larisika, C. Nowak and W. Knoll, *Biosens. Bioelectron.*, 2015, **70**, 21–27.
- 207 F. Buth, D. Kumar, M. Stutzmann and J. Garrido, *Appl. Phys. Lett.*, 2011, **98**, 153302.
- 208 H. Shekhar, V. Chathapuram, S. H. Hyun, S. Hong and H. J. Cho, *presented in part at the Proceedings of IEEE Sensors*, Toronto, Canada, October 22–24, 2003.